



UNIVERSITY OF ILLINOIS  
URBANA

RECEIVED  
NOV 6 2 31 PM '67  
OFFICE OF GRANTS &  
RESEARCH CONTRACTS

# AERONOMY REPORT NO. 11

## PLASMA PROBE STUDIES

by  
K. G. Balmain

May 1, 1966

N67-40306  
(ACCESSION NUMBER)  
100  
(PAGES)  
CR-89781  
(NASA CR OR TMX OR AD NUMBER)

FACILITY FORM 602

(THRU)

1  
(CODE)

25  
(CATEGORY)

Supported by  
National Aeronautics and  
Space Administration  
Grant NsG-511

Aeronomy Laboratory  
Department of Electrical Engineering  
University of Illinois  
Urbana, Illinois

AERONOMY REPORT NO. 11

PLASMA PROBE STUDIES

by

K. G. BALMAIN

May 1, 1966

Supported by  
National Aeronautics and  
Space Administration  
Grant NSG-511

Aeronomy Laboratory  
Department of Electrical Engineering  
University of Illinois  
Urbana, Illinois

#### ACKNOWLEDGMENT

The author acknowledges many helpful discussions with Professor S. A. Bowhill and Dr. J. E. C. Gliddon. He wishes to thank Mr. P. E. Sticha for his numerical computations and Mr. R. J. Kostelnicek for his contributions to the laboratory plasma experiment.

The research was supported by the National Aeronautics and Space Administration under grant NsG-511 and, in part, by the Air Force Cambridge Research Laboratories, Office of Aerospace Research, under contract AF 19(628)-3900.

## ABSTRACT

This report contains five studies of problems relating to RF and DC probes in plasma media with emphasis on the ionospheric plasma. The studies are arranged in five chapters and the material in each chapter is essentially self-contained.

In Chapter 1, the radio frequency impedance of a plasma probe is studied for the case of a collapsed ion sheath resulting from the application of positive DC bias; with sheath collapse the electron density in the plasma is approximately uniform but electrons are continually absorbed into the metal surface of the probe. This absorption is taken into account by using a two-sided velocity distribution function in the Boltzmann transport equation to find the impedance of parallel plate electrodes in a warm plasma. The same impedance formula is derived from the plasma hydrodynamic equations through the application of a boundary condition relating electron velocity and density. This condition is also used to solve the spherical probe impedance problem. At zero frequency all the impedance formulas reduce to the slope of a Langmuir probe characteristic and at zero temperature, the formulas give the familiar cold plasma result. For finite temperatures, the absorptive boundary condition gives an impedance with a positive real part at all frequencies, even in the absence of collisions. Furthermore, the absorptive boundary can cause the disappearance of the low frequency resonance which has been associated with the "resonance probe" direct current peak.

In Chapter 2, quasi-static theory is used to obtain a formula for the impedance of a small spherical electrode in a cold, magnetized plasma. The



derivation allows for the presence of an ion sheath, represented by a free-space gap between the probe and the surrounding plasma.

In Chapter 3, the problem considered is that of a narrow slot antenna in a perfectly conducting, rigid metal plane immersed in a compressible plasma. Expressions are derived for the far fields which consist of an electromagnetic space wave, an electroacoustic space wave and a surface wave. The electroacoustic space wave radiation pattern exhibits two very sharp lobes in directions nearly broadside to the conducting plane. The electromagnetic space wave radiation pattern has a null in the direction parallel to the conducting plane. The surface wave carries a large fraction of the total radiated power and thus it could contribute appreciably to the real part of the slot admittance.

In Chapter 4, a study is made of ion collection at high gas pressure by a spherical DC probe. It is assumed in the theoretical development that the ion drift velocity is proportional to the electric field strength raised to an arbitrary power. The theoretical current-voltage characteristic is used to obtain an ion density profile for a pre-sunrise rocket shot into the lower ionosphere. Some aspects of the theory are verified by measurements on a spherical probe in a laboratory plasma.

In Chapter 5, suggestions are made for future experimental probe studies which can be carried out with the help of ionospheric rockets.

## TABLE OF CONTENTS

	Page
1. IMPEDANCE OF A RADIO FREQUENCY PLASMA PROBE WITH AN ABSORPTIVE SURFACE	1
1.1 Introduction	1
1.2 Parallel Plate Electrodes	5
1.3 Hydrodynamic Analysis of Parallel Plates	11
1.4 Spherical Electrode	14
1.5 Numerical Calculations	17
1.6 Application to Resonance Probes	21
1.7 Conclusions	22
2. IMPEDANCE OF A SPHERICAL PROBE IN A MAGNETOPLASMA	23
2.1 Derivation of the Impedance Formula	23
3. RADIATION FROM A SLOT ANTENNA IN A COMPRESSIBLE PLASMA	28
3.1 Introduction	28
3.2 General Field Analysis	28
3.3 Far Field Solution	38
3.3.1 The Space Waves	38
3.3.2 The Surface Wave	46
3.4 Discussion of Results	49
4. ION COLLECTION BY A SPHERICAL DC PROBE AT HIGH PRESSURES	52
4.1 Introduction	52
4.2 A General Spherical Probe Theory	54
4.3 Probe Measurements in the Ionosphere	60
4.3.1 Collisionless Theory	60
4.3.2 Validity of the Theory	63

## TABLE OF CONTENTS (continued)

	Page
4.3.3 High Pressure Velocity Dependence	65
4.3.4 Results of Pre-Sunrise Flight 14.144 at Wallops Island, Virginia	70
4.3.5 Zero Space Charge Theory	73
4.4 Probe Measurements in the Laboratory	74
5. FUTURE IONOSPHERIC PROBE EXPERIMENTS	81
5.1 Introduction	81
5.2 Experimental Techniques	83
5.2.1 Langmuir Probe	83
5.2.2 Transient Response	85
5.2.3 Impedance Probe	86
5.2.4 Resonance Probe (Resonance Rectification)	87
5.2.5 Probe Configurations	87
5.3 Experimental Program	88
REFERENCES	89

## LIST OF ILLUSTRATIONS

Figure		Page
1.1	The parallel plate electrodes.	4
1.2	Spherical probe resistance and reactance functions for an absorptive surface (ion sheath collapsed).	18
1.3	Spherical probe resistance and reactance functions for a rigid surface (ion sheath present).	19
3.1	The infinitely long, narrow slot in an infinite, conducting plane.	29
3.2	Integration contours.	37
3.3	Space wave radiation patterns.	41
3.4	A comparison of power radiated in the three modes.	48
3.5	Surface wave penetration heights.	50
4.1	The Debye-Huckel sheilding length.	61
4.2	The quantity $(-\alpha^2)$ arising in the theory of the spherical space-charge-limited diode.	62
4.3	Validity limits for the theories.	64
4.4	Altitude of transition from high-field to low-field ion motion.	66
4.5	Measured ion current in the ionosphere.	68
4.6	Ion density profiles.	69
4.7	Electron density as measured by conical nose probe.	71
4.8	Electron-collection curves for a spherical probe in a laboratory plasma.	75
4.9	Ion-collection curves for a spherical probe in a laboratory plasma.	76
4.10	Laboratory gas discharge apparatus.	78
4.11	Brush cathode discharge tube with spherical probes.	79

## 1. IMPEDANCE OF A RADIO FREQUENCY PLASMA PROBE WITH AN ABSORPTIVE SURFACE

### 1.1 Introduction

The small-signal impedance of a radio frequency probe in a warm (compressible) plasma has been discussed by several authors including Hall (1963), Fejer (1964), Wait (1964), and Balmain (1965). In these papers the hydrodynamic equations were used and the probe surface was considered to be essentially rigid, reflecting all particles coming into contact with it. When applied at the probe surface, this rigid boundary condition is a crude but sometimes useful representation for a thin ion sheath, a region of highly nonuniform electron density whose electrostatic field repels almost all electrons coming within a few Debye lengths of the probe surface; a much better sheath representation results when the rigid boundary condition is applied at the sheath edge. Unfortunately, the "sheath edge" is difficult to define and, furthermore, the effective size of the sheath region is difficult to determine experimentally, especially in the case of a rocket or satellite probe in the ionosphere. As a consequence, it is difficult to relate the measured impedance to the properties of the plasma surrounding the probe.

The electron density can be made more nearly uniform by applying to the probe a positive DC bias just sufficient to bring the probe potential up to space potential, a point which can be identified approximately from an examination of the DC current-voltage characteristic; this steady state condition will be referred to as "sheath collapse". The sheath collapse condition has been studied by Wasserstrom, et al. (1965) who note that there is no potential gradient anywhere in the sheath region when the probe potential is equal to the space potential. Under this condition they conclude that there

exists a gradient in electron density which is accompanied by a steady electron flux toward the probe; when collisions are infrequent the electron density gradient is small, the density at the surface of a spherical probe being one-half the ambient density. This analysis suggests an approximate steady state model in which the electron density is constant adjacent to the probe.

Evidently DC bias can help to solve the nonuniform electron density problem but also it can create new problems arising from the direct contact between the electron gas and the metal surface of the probe. Almost all the electrons striking the metal surface are absorbed, an effect which gives rise to the familiar Langmuir probe current-voltage characteristic. In fact, the slope of the Langmuir probe characteristic has been used by Mlodnosky and Garriott (1962) to obtain a probe impedance formula valid at very low frequencies. At higher frequencies (those approaching plasma frequency) little is known about probe impedance under conditions of sheath collapse. In this paper an attempt is made to derive an absorptive surface theory which will give some indication of sheath collapse effects over a wide range of frequencies.

In general, the problem is that of understanding the behavior of a gas in contact with a metal surface. Mott-Smith (1954) made the observation that the hydrodynamic equations are inadequate to derive boundary conditions and, instead, the distribution functions of statistical mechanics must be utilized. Furthermore, he observed that, close to a surface, a gas would have a velocity distribution which is discontinuous in velocity space. That is, the particles in the gas would be subdivided into two groups, those just

emitted from the surface and those about to collide with it; the classification of any one particle would be determined by the direction of its velocity vector. This concept was given concrete form by Lees (1959, 1965) who proposed the use of the following "two-stream Maxwellian" distribution  $F(\bar{r}, \bar{w}, t)$ : if region "a" of velocity space contains the emitted particles and region "b" contains the incident particles, then in region "a",

$$F(\bar{r}, \bar{w}, t) = F_a(\bar{r}, \bar{w}, t) = n_a(\bar{r}, t) \left[ \frac{m}{2\pi k T_a(\bar{r}, t)} \right]^{3/2} \exp \left[ -\frac{m |\bar{w} - u_a(\bar{r}, t)|^2}{2 k T_a(\bar{r}, t)} \right]$$

and in region "b"

$$F(\bar{r}, \bar{w}, t) = F_b(\bar{r}, \bar{w}, t) = n_b(\bar{r}, t) \left[ \frac{m}{2 \pi k T_b(\bar{r}, t)} \right]^{3/2} \exp \left[ -\frac{m |\bar{w} - u_b(\bar{r}, t)|^2}{2 k T_b(\bar{r}, t)} \right]$$

in which  $k$  is Boltzmann's constant and  $\bar{w}$  is a vector denoting the particle velocity. The quantities  $n_a$ ,  $n_b$ ,  $\bar{u}_a$ ,  $\bar{u}_b$ ,  $T_a$ ,  $T_b$  constitute ten undetermined functions of space and time, functions which are "weighted" by arranging them in Maxwellian form. Since the form of the distribution function is assumed, this function is likely to be useful only in the sense of an average over velocity space. For this reason it is appropriate to use the two-sided Maxwellian distribution in the Boltzmann transport equation whose various moments yield differential equations in the undetermined functions.

In general, a finite number of moment equations is sufficient to solve any given problem. Unfortunately, there is no mathematical means of deciding which moment equations to use; the only recourse is to make use of those

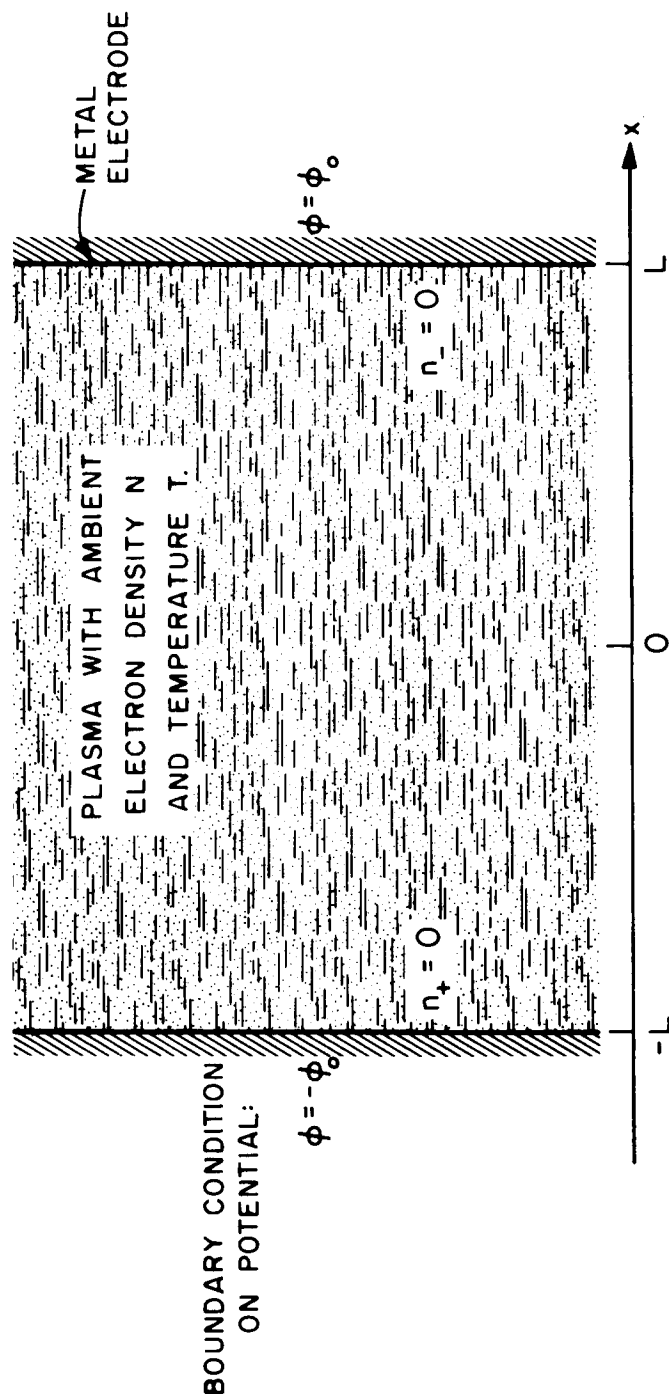


Figure 1.1 The parallel plate electrodes.



moments whose physical interpretations are most meaningful in the problem under consideration. In recent years the two-sided Maxwellian method has been applied to gas flow (Liu and Lees, 1961), to heat transfer (Lees and Liu, 1962), and to electrostatic probes (Wasserstrom, et al., 1965).

The problem at hand is that of an electron gas in contact with a completely absorptive surface, that is, a surface from which no particles are emitted. If region "a" in velocity space contains the emitted particles, then the absorptive boundary condition must be  $n_a = 0$ . Due to this boundary condition,  $n_a$  and  $n_b$  are likely to be the most significant of the undertermined functions. In order to keep the analysis as simple as possible, we shall follow Wasserstrom, et al. and set  $T_a(\vec{r}, t) = T_b(\vec{r}, t) = T$  (isothermal approximation) and  $\bar{u}_a(\vec{r}, t) = \bar{u}_b(\vec{r}, t) = 0$ ; the latter restriction does not preclude particle flux which can still arise from the difference between  $n_a$  and  $n_b$ . This approach will be employed in the following impedance analysis of parallel plate and spherical electrodes in a uniform, warm plasma containing mobile electrons and immobile ions. Although  $\bar{u}_a$  and  $\bar{u}_b$  are not included in the analysis, it is nevertheless possible that their inclusion could affect the results appreciably.

## 1.2 Parallel Plate Electrodes

The parallel plate geometry shown in Figure 1.1 is very simple in that only one coordinate,  $x$ , is involved. The geometry suggests a division of velocity space into two parts determined by the sign of  $w_x$ , the  $x$  component of electron velocity. Furthermore, for small, sinusoidal oscillations all the quantities of interest may be separated into steady and oscillating parts. Thus  $n_a(x, t)$  may be expressed as  $N_+(x) + n_+(x)e^{j\omega t}$  for  $w_x > 0$  and

$n_b(x,t)$  may be expressed as  $N_-(x) + n_-(x)e^{j\omega t}$  for  $w_x < 0$ . Consequently the velocity distribution function  $F(x,\bar{w},t)$  takes the form  $f_0(x,\bar{w}) + f(x,\bar{w})e^{j\omega t}$  in which  $f$  is given by

$$f(x,\bar{w}) = f_+(x,\bar{w}) = n_+(x) \left(\frac{m}{2\pi kT}\right)^{3/2} e^{-\frac{mw^2}{2kT}}, \quad w_x > 0, \quad (1)$$

$$f(x,\bar{w}) = f_-(x,\bar{w}) = n_-(x) \left(\frac{m}{2\pi kT}\right)^{3/2} e^{-\frac{mw^2}{2kT}}, \quad w_x < 0. \quad (2)$$

In addition, the electric field strength is entirely in the  $x$  direction and is given by  $E_0(x) + E(x)e^{j\omega t}$ . Under conditions of sheath collapse, however, there is no steady potential gradient and  $E_0(x) = 0$ . As mentioned in the introduction, the collapsed-sheath electron density will be assumed to be uniform.

The zero order and first order moments of the Boltzmann transport equation are physically suitable for the analysis because they represent, respectively, conservation of particles and conservation of momentum. If  $e$  is the electron charge magnitude, the moment equations may be expressed as follows in terms of integrals over velocity space:

$$j\omega \int f d\bar{w} + \frac{d}{dx} \int w_x f d\bar{w} = 0 \quad (3)$$

$$j\omega \int w_x f d\bar{w} + \frac{d}{dx} \int w_x^2 f d\bar{w} + \frac{e}{m} E \int f_0 d\bar{w} = -v \int w_x f d\bar{w} \quad (4)$$

The collisional term in (3) is zero because collisions cannot change the number of particles per unit volume (Spitzer, 1962). The collisional term

in (4) is obtained from the simplified model discussed by Bhatnagar, et al. (1954). This model defines the collisional frequency between electrons and heavy particles  $\nu$  which is considered here to be independent of velocity.

The integrals in (3) and (4) may be evaluated as follows using (1) and (2):

$$\int f_0 d\bar{w} = N = \text{steady ambient electron density} \quad (5)$$

$$\int f d\bar{w} = 1/2(n_+ + n_-) = n = \text{oscillating electron density} \quad (6)$$

$$\int w_x f d\bar{w} = \sqrt{\frac{kT}{2\pi m}} (n_+ - n_-) = \Gamma = \text{oscillating electron flux} \quad (7)$$

$$\int w_x^2 f d\bar{w} = \frac{kT}{2m} (n_+ + n_-) \quad (8)$$

The next approximation is that  $E$  may be represented as the gradient of a scalar potential,

$$E = - \frac{d\phi}{dx} \quad (9)$$

Thus  $\phi$  must satisfy Poisson's equation which is

$$\frac{d^2\phi}{dx^2} = \frac{ne}{\epsilon_0} \quad (10)$$

The two moment equations and Poisson's equation with the three unknowns  $n_+$ ,  $n_-$  and  $\phi$  now may be solved provided that four boundary conditions can

be established (four arbitrary constants arise in the solution of one second order and two first order differential equations). The conditions on the potential need no explanation, but the conditions on  $n_+$ ,  $n_-$  express the idea that no electrons are emitted from the two electrode surfaces. The boundary conditions are

$$\begin{aligned}\phi(-L) &= -\phi_0, \quad n_+(-L) = 0, \\ \phi(L) &= \phi_0, \quad n_-(L) = 0.\end{aligned}\tag{11}$$

It is convenient at this point to introduce the following set of simplifying definitions and normalizations:

$$\begin{aligned}\frac{v}{\omega} &= Z, \quad U = 1 - jZ, \quad \frac{Ne^2}{m\epsilon_0} = \omega_N^2, \quad \frac{\omega_N^2}{\omega^2} = X \\ \sqrt{\frac{\epsilon_0 kT}{Ne^2}} &= \lambda_D, \quad \frac{x}{\lambda_D} = \xi, \quad \frac{L}{\lambda_D} = h, \quad \frac{e\phi}{kT} = \phi_1, \\ \frac{n_+ + n_-}{N} &= N_1, \quad \frac{n_+ - n_-}{N} = N_2.\end{aligned}\tag{12}$$

The differential equations (3), (4) and (10) now may be expressed as

$$j\sqrt{\frac{\pi}{2}} X^{-1/2} N_1 + \frac{dN_2}{d\xi} = 0\tag{13}$$

$$j\sqrt{\frac{2}{\pi}} U X^{-1/2} N_2 + \frac{dN_1}{d\xi} - 2\frac{d\phi_1}{d\xi} = 0\tag{14}$$

$$\frac{d^2 \phi_1}{d\xi^2} = 1/2 N_1 . \quad (15)$$

Differentiation of (14) and elimination of  $N_2$  and  $\phi_1$  using (13) and (15) give the differential equation

$$\frac{d^2 N_1}{d\xi^2} - \alpha^2 N_1 = 0 \quad (16)$$

in which  $\alpha^2 = 1 - UX^{-1}$ . The solution to (16) is

$$N_1 = Ae^{\alpha\xi} + Be^{-\alpha\xi} \quad (17)$$

in which A and B are arbitrary constants.

Integration of (13) and (14) now yields

$$N_2 = -j \sqrt{\frac{\pi}{2}} (X - U)^{-1/2} (Ae^{\alpha\xi} - Be^{-\alpha\xi}) + C \quad (18)$$

$$n_1 - 2\phi_1 = -j \sqrt{\frac{2}{\pi}} \frac{U}{X^{1/2}} \left[ -j \sqrt{\frac{\pi}{2}} \frac{X^{1/2}}{X - U} (Ae^{\alpha\xi} + Be^{-\alpha\xi}) + C\xi \right] + D \quad (19)$$

in which C and D are additional arbitrary constants. The boundary conditions permit expression of B, C and D in terms of A.

$$B = -A , \quad D = 0 ,$$

$$C = A \left[ e^{\alpha h} - e^{-\alpha h} + j \sqrt{\frac{\pi}{2}} (X - U)^{-1/2} (e^{\alpha h} + e^{-\alpha h}) \right] \quad (20)$$

It is unnecessary to evaluate A since it cancels out in the impedance calculation.

The input impedance of parallel plates with area S may be expressed as

$$Z_{in} = - \frac{2\phi}{S(J_p + J_d)} \bigg|_{x=L} \quad (21)$$

in which  $J_p$  and  $J_d$  are respectively the particle and displacement current densities given by

$$J_p = -e\Gamma, \quad (22)$$

$$J_d = -j\omega\epsilon_0 \frac{d\phi}{dx}. \quad (23)$$

After some algebraic manipulation, (21) reduces to

$$Z_{in} = \frac{2L}{j\omega\epsilon_0 K_0 S} \left[ 1 - \frac{X}{U} \left\{ \alpha h (\coth \alpha h - j \sqrt{\frac{2}{\pi}} X^{1/2} \alpha) \right\}^{-1} \right] \quad (24)$$

in which  $K_0 = 1 - XU^{-1}$  and is the relative permittivity of a cold plasma.

Equation (24) would be identical to the rigid boundary impedance formula derived by Hall (for the collisionless case) if the term  $-j \sqrt{\frac{2}{\pi}} X^{1/2} \alpha$  were not present. It is this term which arises from the absorptive boundary condition and gives  $Z_{in}$  a positive real part even when the collision frequency is zero.

It is interesting to examine some limiting cases, especially the zero temperature and zero frequency limits. As  $T \rightarrow 0$ ,  $h \rightarrow \infty$  and the familiar cold plasma impedance expression remains. In the limit as  $\omega \rightarrow 0$ , (24) becomes

$$Z_{in} = \frac{2L}{\epsilon_0} \frac{\nu}{S\omega_N} \left( 1 + \sqrt{\frac{\pi}{2}} \frac{\omega_N}{\nu h} \right) \quad (25)$$

As the collision frequency  $\nu$  in (25) increases, the relative importance of the absorptive boundary condition decreases. On the other hand as  $\nu \rightarrow 0$  in (25), the impedance becomes

$$Z_{in} = \frac{\sqrt{2\pi mk'T}}{Ne^2 S} \quad (26)$$

which is one-half the resistance given by the formula of Mlodnosky and Garriott (1962) at the point of sheath collapse; their formula was derived by taking the slope of the DC Langmuir probe characteristic.

### 1.3 Hydrodynamic Analysis of Parallel Plates

Radio frequency plasma probes frequently have been analyzed using the hydrodynamic equations in a form applicable to a plasma with constant ambient electron density and zero steady drift velocity. In general, in these analyses the ion sheath has been represented by the rigid boundary condition applied at the probe surface. It is worthwhile at this point to seek a simple, approximate modification to this theory which will give some indication of the change in impedance which occurs when the sheath is collapsed.

For the one-dimensional case the hydrodynamic equations are

$$j\omega m N v = - Ne E - \gamma k T \frac{dn}{dx} - \nu m N v \quad (27)$$

$$N \frac{dv}{dx} = - j \omega n \quad (28)$$

in which  $v$  is the electron velocity and  $\gamma$  is the ratio of specific heats.

These equations may be simplified by the use of (12) together with

$$\frac{kT}{m} = V^2, \quad \frac{v}{V} = v_1, \quad \frac{n}{N} = n_1 \quad (29)$$

With the inclusion of (9), the hydrodynamic equations and Poisson's equation may be expressed as

$$jX^{-1/2}n_1 + \frac{dv_1}{d\xi} = 0 \quad (30)$$

$$jUX^{-1/2}v_1 + \gamma \frac{dn_1}{d\xi} - \frac{d^2\phi}{d\xi^2} = 0 \quad (31)$$

$$\frac{d^2\phi}{d\xi^2} = n_1 \quad (32)$$

Equations (30), (31) and (32) are identical in form to (13), (14) and (15); consequently the same procedure may be used in obtaining the solution of the parallel plate problem. All that remains is the inclusion of boundary conditions which take into account the absorption of electrons at the electrode surfaces.

The boundary conditions on potential are the same as before but two additional conditions must be found in order to complete the solution of (30), (31) and (32); these conditions may be derived from (6) and (7). Note that  $n_+(-L) = 0$  and that  $n_-(-L)$  may be eliminated from (6) and (7) to give

$$\Gamma(-L) = -2n(-L) \sqrt{\frac{kT}{2\pi m}} \quad (33)$$



Thus at the boundary, the oscillating electron flux is directly proportional to the oscillating electron density. Within the framework of the constant-density, drift-free hydrodynamic theory, the oscillating electron flux is expressed as

$$\Gamma(x) = Nv(x) . \quad (34)$$

Combining (33) and (34) and normalizing gives the boundary condition

$$v_1(-L) = -a n_1(-L) \quad (35)$$

in which  $a = (2/\pi)^{1/2}$ . Similarly,

$$v_1(L) = a n_1(L) . \quad (36)$$

The quantity "a" serves as an "absorption coefficient" since setting it equal to zero is equivalent to assuming a rigid or reflecting boundary. It should be pointed out that the electroacoustic Poynting vector is proportional to  $n v^*$  (Hessel, et al., 1962) and therefore the conditions (35) and (36) indicate absorption of radio frequency power by the electrode surfaces.

The parallel plate impedance expression may be found as before and is given by

$$Z_{in} = \frac{2L}{j\omega\epsilon_o K_o S} \left[ 1 - \frac{X}{U} \left\{ \alpha_1 h (\coth \alpha_1 h - jaX^{1/2} \alpha_1) \right\}^{-1} \right] \quad (37)$$

in which  $\alpha_1 = \gamma^{-1/2} \alpha$ . Under isothermal conditions ( $\gamma = 1$ ), (37) is identical to (24). This does not imply that the two-sided distribution technique and the hydrodynamic equation technique will always give the same result in other geometries; it does suggest, however, that the results will be similar. The value of  $\gamma$  may be estimated from the work of Pavkovich (1964) who concludes that, below plasma frequency,  $\gamma$  varies regularly with frequency, increasing from 1 at  $\omega = 0$  to 3 at  $\omega = \omega_N$ ; since the most pronounced impedance effects are expected at frequencies appreciably below plasma frequency (Fejer, 1964), the value  $\gamma = 1$  would seem to be a suitable choice for approximate calculations.

#### 1.4 Spherical Electrode

The single spherical electrode is the simplest structure which exhibits the radiation of electroacoustic waves as was demonstrated by Fejer (1964) using the rigid boundary condition. The following analysis is similar to Fejer's, but employs the absorptive boundary condition. If  $r$  is radial distance and if  $\rho$  is the normalized distance defined by

$$\frac{r}{\lambda_D} = \rho \quad (38)$$

then the hydrodynamic equations and Poisson's equation may be expressed as

$$jX^{-1/2} n_1 + \frac{1}{\rho^2} \frac{d}{d\rho} (\rho^2 v_1) = 0 \quad (39)$$

$$jUX^{-1/2} v_1 + \gamma \frac{dn_1}{d\rho} - \frac{d\phi_1}{d\rho} = 0 \quad (40)$$

$$\frac{1}{\rho^2} \frac{d}{d\rho} (\rho^2 \frac{d\phi_1}{d\rho}) = n_1 \quad (41)$$

The probe surface is defined by  $r = r_0$ , or in normalized form,  $\rho = \rho_0$ ; thus  $\rho_0$  is the probe radius in Debye lengths. The boundary conditions are

$$\begin{aligned}\phi(\rho_0) &= \phi_0, & v_1(\rho_0) &= -a n_1(\rho_0), \\ \phi(\infty) &= 0, & v_1(\infty) &= n_1(\infty) = 0.\end{aligned}\quad (42)$$

The solution to the impedance problem follows in a manner similar to the parallel plate solution.

From equations (39) to (41), one may derive

$$\frac{1}{\rho^2} \frac{d}{d\rho} \left( \rho^2 \frac{dn_1}{d\rho} \right) - \alpha_1^2 n_1 = 0. \quad (43)$$

The solution to (43) which decays with increasing radial distance has the form

$$n_1 = A \frac{e^{-\alpha_1 \rho}}{\rho} \quad (44)$$

in which A is an arbitrary constant. Note that the square root represented by  $\alpha_1$  must be chosen to have a positive real part. Integration results in the expressions

$$v_1 = A j X^{-1/2} \frac{1 + \alpha_1 \rho}{\alpha_1^2 \rho^2} e^{-\alpha_1 \rho} + \frac{B}{\rho^2} \quad (45)$$

$$\gamma n_1 - \phi_1 = j \frac{U X^{-1/2}}{\alpha_1} (A j X^{-1/2} \frac{e^{-\alpha_1 \rho}}{\alpha_1 \rho} + \frac{\alpha_1 B}{\rho}) + C. \quad (46)$$

The arbitrary constants B and C may be evaluated using the boundary conditions. Thus,

$$C = 0$$

$$B = -A\rho_o^2 (jX^{-1/2} \frac{1 + \alpha_1 \rho_o}{\alpha_1^2 \rho_o^2} + \frac{a}{\rho_o}) e^{-\alpha_1 \rho_o}. \quad (47)$$

The probe impedance may be determined in a straightforward way from the formula

$$Z_{in} = \frac{\phi}{4\pi r_o^2 (J_p + J_d)} \bigg|_{\rho = \rho_o}. \quad (48)$$

After algebraic manipulation, the impedance expression emerges as

$$Z_{in} = \frac{1}{j\omega 4\pi r_o^2 \epsilon_o K_o} \left[ 1 - \frac{X}{U} (1 + \alpha_1 \rho_o - jaX^{1/2} \alpha_1^2 \rho_o)^{-1} \right]. \quad (49)$$

With  $a = 0$  the impedance is the same as that derived by Fejer (1964). As in (24) and (37) the term containing "a" arises directly from the use of the absorptive boundary condition. The term  $\alpha_1 \rho_o$  contributes a positive real part to  $Z_{in}$  when  $v = 0$  and  $\omega > \omega_N$ ; this arises from the radiation of electro-acoustic waves.

In the limit as  $\omega \rightarrow 0$  the above impedance formula reduces to

$$Z_{in} = \frac{v}{4\pi r_o^2 \epsilon_o \omega_N} \left( 1 + \frac{\gamma \omega_N}{av \rho_o} \right) \quad (50)$$

and for the collisionless case, it becomes

$$Z_{in} = \frac{\gamma}{2} \frac{\sqrt{2\pi mkT}}{4\pi r_o^2 Ne^2} \quad (51)$$

At zero frequency, the isothermal approximation applies and thus  $\gamma = 1$ . The assumption of an idealized, constant-density, drift-free steady state introduces an error which may be estimated by comparing the above formula with a corresponding one derived by Wasserstrom, et al. (1965). For small perturbations about space potential they derive the impedance expression

$$Z_{in} = (1 + \ln 2) \frac{\sqrt{2\pi mkT}}{4\pi r_o^2 Ne^2} \quad (52)$$

The decrease in electron density near the probe to one-half its ambient value accounts for the greater part of the difference between (51) and (52).

### 1.5 Numerical Calculations

The spherical electrode impedance result is used in the numerical calculations because it includes the effects of electroacoustic radiation. Isothermal, collisionless conditions are assumed ( $\gamma = 1$ ,  $U = 1$ ) and the impedance is expressed as a function of normalized frequency defined by

$$\psi = \frac{\omega}{\omega_N} \quad (53)$$

The impedance may be expressed in terms of the resistance and reactance functions  $F_R$  and  $F_X$  defined such that at  $T = 0$ ,  $F_R = 0$  and  $F_X = 1$  at all frequencies. The impedance expressions are, for  $\psi \leq 1$ ,

$$\omega 4\pi r_o^2 \epsilon_o Z_{in} = j \frac{\psi^2}{1 - \psi^2} \left[ 1 - \frac{1}{\psi^2 (1 + \sqrt{1 - \psi^2} \rho_o) - ja\psi(1 - \psi^2)\rho_o} \right] \quad (54)$$

$$= \frac{\psi^2}{1 - \psi^2} \left[ F_R + jF_X \right] \quad (55)$$

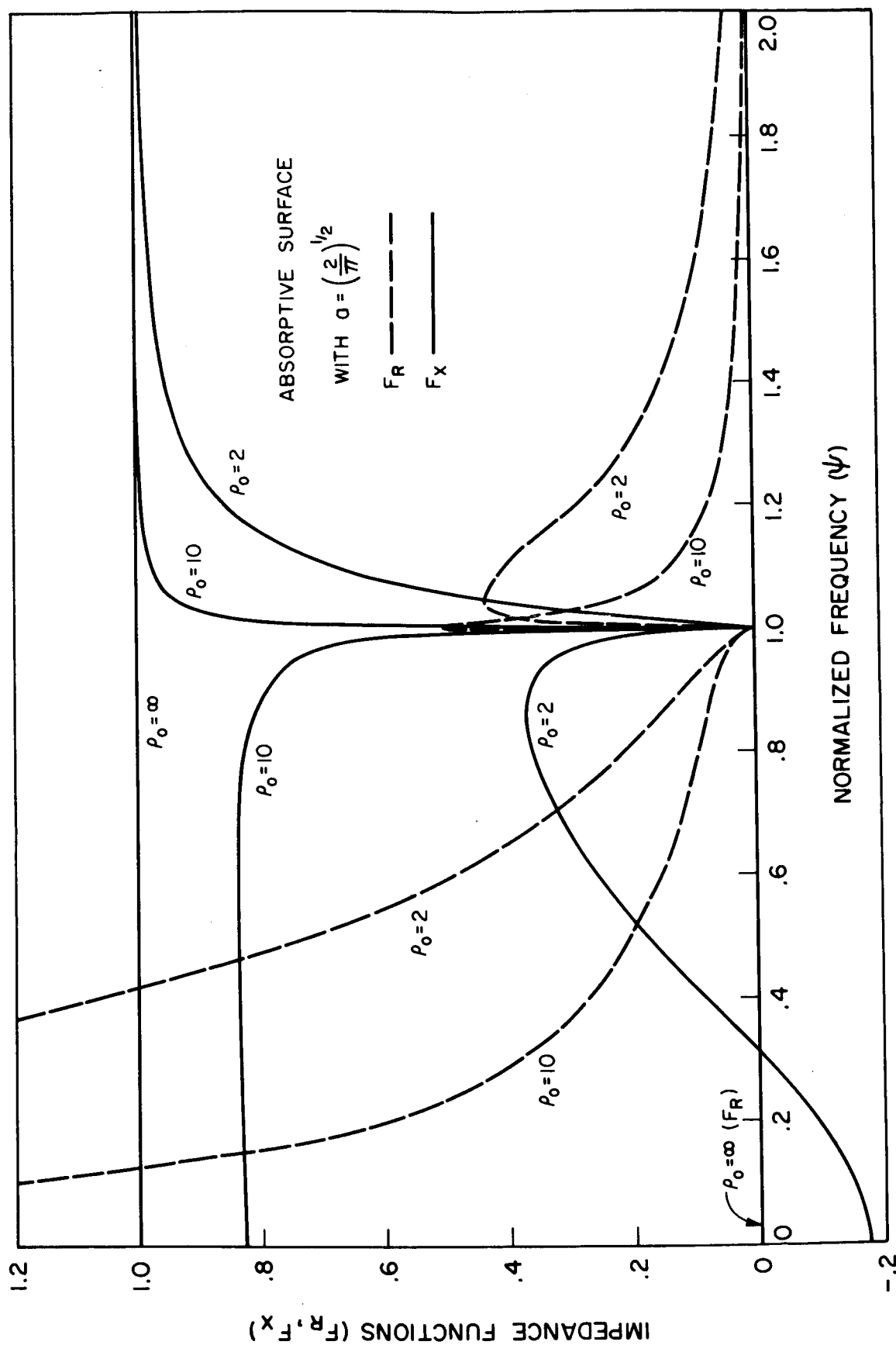


Figure 1.2 Spherical probe resistance and reactance functions for an absorptive surface (ion sheath collapsed).

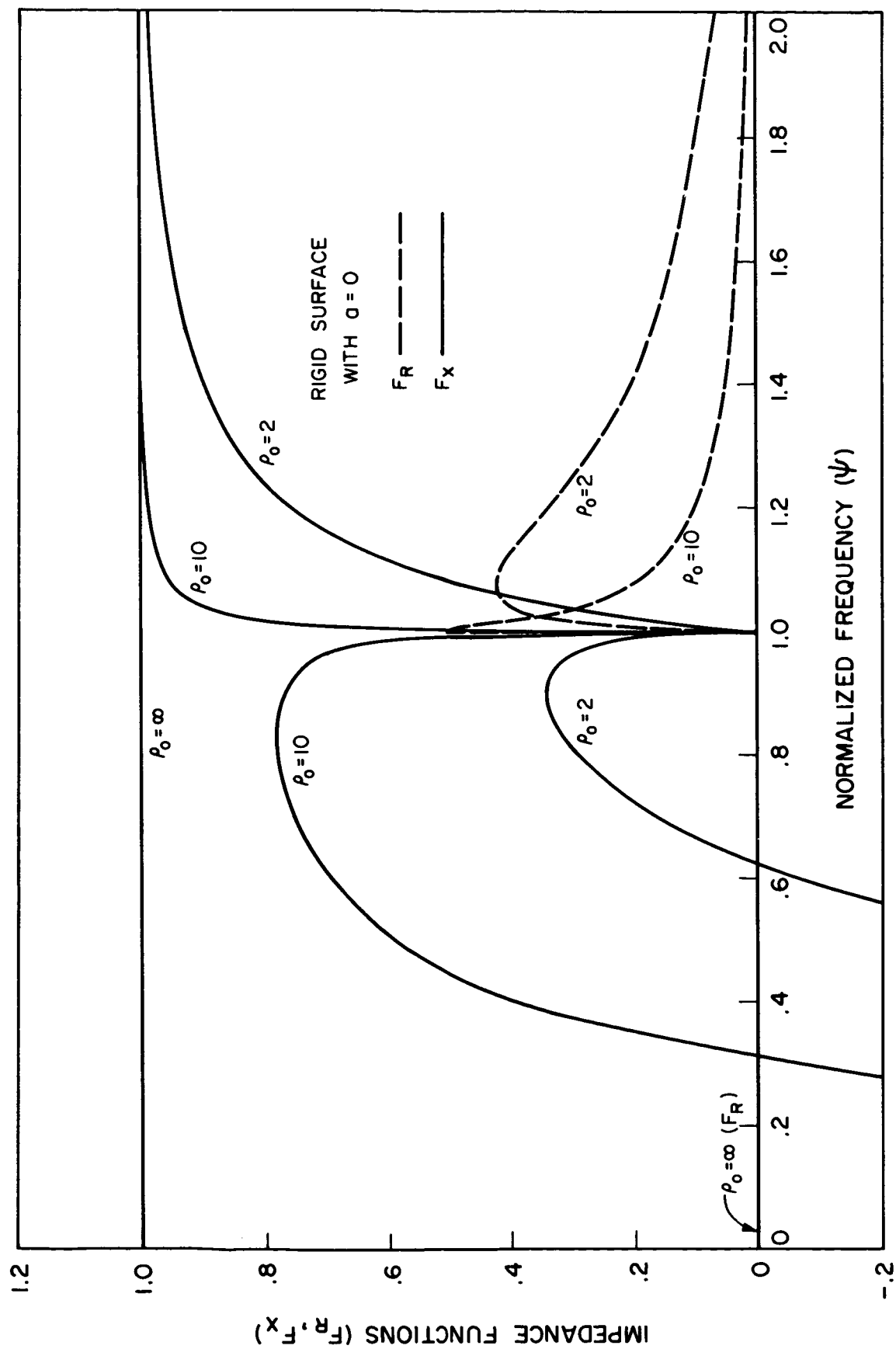


Figure 1.3 Spherical probe resistance and reactance functions for a rigid surface (ion sheath present).

and for  $\psi \geq 1$ ,

$$4\pi r_o \epsilon_o Z_{in} = -j \frac{\psi^2}{\psi^2 - 1} \left[ 1 - \frac{1}{\psi^2 + j\rho_o \left\{ \psi^2 \sqrt{\psi^2 - 1} + a\psi (\psi^2 - 1) \right\}} \right] \quad (56)$$

$$= \frac{\psi^2}{\psi^2 - 1} \left[ F_R - jF_X \right]. \quad (57)$$

The functions  $F_R$  and  $F_X$  are shown in Figures 1.2 and 1.3 for absorptive and rigid boundaries, respectively. The rigid boundary condition is very limited in its applicability but it should give a useful result for a thin ion sheath (one to two Debye lengths thick). Thus the transition from  $a = 0$  to  $a = (2/\pi)^{1/2}$  should give at least a qualitative picture of impedance behavior as the ion sheath is collapsed. A comparison of Figures 1.2 and 1.3 shows that the surface absorptivity has little effect at frequencies above the plasma frequency. The most pronounced effects occur below plasma frequency where, fortunately, the isothermal approximation is most likely to be valid. In this frequency range, collapse of the ion sheath brings the reactance closer to the value predicted by cold plasma theory. However, sheath collapse is accompanied by the introduction of a resistive effect which is especially important at very low frequencies. The low frequency resonance ( $F_X = 0$ ) disappears with sheath collapse provided that the probe radius is greater than approximately three Debye lengths.



### 1.6 Application to Resonance Probes

The resonance probe phenomenon consists of the appearance of a peak in the direct current to an RF probe as the frequency is varied; the subject has been reviewed thoroughly by Crawford and Mlodnosky (1964), Harp and Crawford (1964), and by Crawford and Harp (1965). In order to determine whether or not the absorptive boundary theory sheds any light on the resonance probe phenomenon, one may examine the oscillating electron density at the surface of a spherical probe for a fixed value of applied voltage.

$$\left. \frac{n_1}{\phi_1} \right|_{\rho = \rho_0} = \left[ \gamma \left( 1 - \frac{UX^{-1/2} \rho_0}{\sqrt{X - U}} \right) + jaUX^{-1/2} \rho_0 \right]^{-1} \quad (58)$$

At zero collision frequency the real part in (58) goes to zero at

$$\frac{X^{-1/2} \rho_0}{\sqrt{X - 1}} = 1. \quad (59)$$

This defines a frequency  $\omega_m$  at which  $n_1$  becomes infinite under rigid boundary conditions ( $a = 0$ ). Under non-linear conditions, it is reasonable to expect a steady current peak at this frequency as suggested by Fejer (1964). With an absorptive boundary (collapsed sheath), the term  $aUX^{-1/2} \rho_0$  in (58) is of the order of unity at  $\omega_m$  and thus the current peak must be very effectively flattened even when the collision frequency is zero.

The resonance probe experiment normally is carried out with a small negative bias on the probe so that only a fraction of the electrons entering the sheath region actually reaches the probe. In such a situation (58) may

still be meaningful provided "a" is allowed to take on some value intermediate between 0 and  $(2/\pi)^{1/2}$ . The present purpose is not to assign a value to "a" but rather to suggest that the surface absorption represented by it could play an important part in determining the height and width of the resonance probe current peak.

### 1.7 Conclusions

Impedance expressions have been derived for parallel plate and spherical electrodes under conditions of ion sheath collapse. These expressions may be somewhat limited in quantitative accuracy because a highly idealized steady state was assumed and because only two undetermined functions were used in the assumed velocity distribution. Nevertheless the absorptive surface theory does lead to the following qualitative conclusions with respect to the effects of ion sheath collapse:

1. The absorption of electrons by the probe is accompanied by the absorption of radio frequency power at all frequencies.
2. Above plasma frequency there is little change in impedance.
3. Below plasma frequency there is a significant change in the impedance which becomes predominantly resistive as the frequency approaches zero.
4. The spherical probe low frequency resonance (zero in reactance) disappears for probe radii greater than about three Debye lengths.
5. The reactance tends to approach the value predicted by cold plasma theory. This effect is especially noticeable if the probe radius is greater than about ten Debye lengths.
6. In the "resonance probe" (or "resonance rectification") effect, the direct current peak is flattened by surface absorption.

## 2. IMPEDANCE OF A SPHERICAL PROBE IN A MAGNETOPLASMA

### 2.1 Derivation of the Impedance Formula

In a recent paper, Balmain (1964) used quasi-static theory to compute the impedance of a short dipole in a magnetoplasma and also discussed the use of a scaling procedure which transforms the free space equations into magnetoplasma equations. It will be shown here how such a scaling procedure can be used to derive an approximate, closed-form expression for the impedance of a small, spherical probe immersed in a cold magnetoplasma.

The basic impedance formula may be set up using some results from elementary electrostatics. The energy necessary to assemble a charge  $Q$  on a conducting body with capacitance  $C$  is

$$W = \frac{1}{2} \frac{Q^2}{C} \quad (1)$$

If the charge has density  $\rho$  and if the conductor potential is  $V$ , the energy is also given by

$$W = \frac{1}{2} \int \rho V \, dv \quad (2)$$

Thus the input impedance of the conducting body for slowly-varying sinusoidal fields may be expressed as

$$Z_{in} = \frac{1}{j\omega C} = \frac{1}{j\omega Q^2} \int \rho V \, dv \quad (3)$$

For a spherical probe, the charge  $\rho$  is spread in a thin layer over the surface of the sphere. If the probe is small, the potential  $V$  may be

approximated by the potential of a point charge of  $Q$  coulombs located at the center of the sphere.

The potential of a point charge in a magnetoplasma may be obtained by scaling. If primes are used to indicate free space coordinates an appropriate scaling is given by

$$x' = \sqrt{K_0 K'} x, \quad y' = \sqrt{K_0 K'} y, \quad z' = K' z. \quad (4)$$

The quantities  $K'$  and  $K_0$  are the diagonal elements of the permittivity tensor and are given by

$$K' = 1 - \frac{XU}{U^2 - Y^2}, \quad K_0 = 1 - \frac{X}{U} \quad (5)$$

in which  $X = \omega_N^2 / \omega^2$ ,  $Y = \omega_H / \omega$ ,  $U = 1 - jZ = 1 - j\nu / \omega$ .

The quantities  $\omega_N$ ,  $\omega_H$  and  $\nu$  are respectively the electron plasma, cyclotron and collision frequencies. Scaling of the free space point charge potential may be carried out as follows:

$$\begin{aligned} V &= \frac{Q}{4\pi\epsilon_0 r'} = \frac{Q}{4\pi\epsilon_0 \sqrt{x'^2 + y'^2 + z'^2}} \\ &= \frac{Q}{4\pi\epsilon_0 \sqrt{K_0 K' x^2 + K_0 K' y^2 + K'^2 z^2}} \end{aligned} \quad (6)$$

The following definitions,  $x = r \sin \theta \cos \phi$ ,  $y = r \sin \theta \sin \phi$ ,  $z = r \cos \theta$ ,  $m^2 = 1 - \frac{K_0}{K'}$ , make it possible to express (6) as

$$V = \frac{Q}{4\pi\epsilon_0 R K' \sqrt{1 - m^2 \sin^2 \theta}} \quad (7)$$

which is the required potential of a point charge in a magnetoplasma.

In order to calculate the impedance, the charge density  $\rho$  must be determined. The total charge of  $Q$  coulombs is spread in a thin layer over the surface of the sphere which has radius  $R$ . If the actual charge distribution is approximated by a uniform distribution, then the charge density may be expressed as

$$\rho = \frac{Q}{4\pi R^2} \delta(r - R) \quad (8)$$

in which  $\delta$  is the Dirac delta. Substitution of (7) and (8) into (3) permits the volume integration to be carried out, giving

$$\begin{aligned} j\omega 8\pi\epsilon_0 K'R Z_{in} &= \int_0^\pi \frac{\sin \theta d\theta}{\sqrt{1 - m^2 \sin^2 \theta}} \\ &= \left[ -\frac{1}{m} \ln \left\{ m \cos \theta + \sqrt{1 - m^2 \sin^2 \theta} \right\} \right]_0^\pi \end{aligned}$$

Thus the impedance formula reduces to

$$Z_{in} = \frac{1}{j\omega 8\pi\epsilon_0 R K' m} \ln \frac{1 + m}{1 - m} \quad (9)$$

in which  $m = \sqrt{1 - \frac{K_0}{K'}}$ . In the above expression, the logarithm must be calculated using the formula

$$\ln w = \ln |w| + j \arg w$$

in which  $-\pi < \arg w < \pi$ .

The influence of an ion sheath may be estimated by representing it as a free space gap of thickness  $S$  separating the probe from the uniform plasma. Thus if the probe radius is  $R$ , the radius of the sheath edge is  $R + S$ . Under these conditions the probe impedance consists of the sheath impedance in series with the plasma impedance, the latter being approximated by (9) with  $R$  replaced by  $R + S$ . If the quantity  $T$  is defined as

$$T = \frac{1}{2K'm} \ln \frac{1+m}{1-m} ,$$

the the probe impedance with an ion sheath present is given by

$$Z_{in} = \frac{1}{j\omega 4\pi\epsilon_0} \left( \frac{1}{R} - \frac{1}{R+S} \right) + \frac{T}{j\omega 4\pi\epsilon_0 (R+S)} = \frac{1}{j\omega 4\pi\epsilon_0 R} \frac{S+R'T}{R+S} . \quad (10)$$

Under lossless conditions ( $Z \rightarrow 0$ ) the above formula has a positive real part when  $K_0/K'$  is negative. This anomalous resistance has been noticed by Kaiser (1962) and Balmain (1964) in their studies of dipole impedance and it arises whenever the quasi-static differential equation is hyperbolic. The impedance is entirely reactive when the differential equation is elliptic, that is when  $K_0/K'$  is positive. Under hyperbolic conditions the anomalous resistance arises from the imaginary part of the logarithm whose sign must be determined by evaluating the logarithm for a small value of  $Z$  and then taking the limit as  $Z \rightarrow 0$ .

Another probe effect of interest is the "resonance rectification" effect in which an RF probe exhibits a direct current peak at a frequency which for isotropic plasmas is below the plasma frequency. It is believed

that the peak in direct current occurs near the minimum in RF impedance. This minimum may be regarded as a "series resonance" due to the series connection of a capacitive sheath region and an inductive plasma region (refer to Crawford (1965) and Dote and Ichimiya (1965) for further discussion). Inspection of (10) indicates that, under lossless conditions, a series resonance (zero in impedance) can occur if  $T$  is negative. The factor  $T$  is dominated by  $K'$  which is negative in the frequency range

$$\omega_H < \omega < \sqrt{\omega_N^2 + \omega_H^2} . \quad (11)$$

Thus rectified current peaks are to be expected mainly within this frequency range.

It must be emphasized that the spherical probe model assumed is highly idealized. In practice the fields would be distorted by the presence of the connecting wires and the nearby reference electrode. In addition, the sheath-plasma interface would not be spherical but would be distorted by the magnetic field. Another important factor is the size of the probe; its radius would have to be much larger than a Debye length to avoid effects arising from the non-zero temperature of the plasma.

### 3. RADIATION FROM A SLOT ANTENNA IN A COMPRESSIBLE PLASMA

#### 3.1 Introduction

Measurements of antenna impedance in a plasma medium frequently have revealed an apparent power loss much greater than that which could arise from electromagnetic radiation and electron-molecule collisions within the gas (Balmain, 1964). A mechanism which might account for part of this power loss is the generation of compressible plasma surface waves of the type found theoretically by Seshadri (1964). Such surface waves would be excited at the "gap" or "terminals" of the antenna and would propagate outward along its surface. Since the surface waves are very rapidly attenuated by collisions, reflections of the waves from the extremities of the antenna would have little effect on the impedance. It is the purpose of this report to compare the power carried off by the surface waves with the power carried off by the electromagnetic and electroacoustic space waves whose radiation patterns will be obtained in the process. The configuration to be studied is the infinitely long, narrow slot antenna immersed in a compressible plasma.

#### 3.2 General Field Analysis

The slot antenna to be studied is shown in Figure 3.1. The fields are assumed not to vary in the  $z$  direction and the metal plane is assumed to be perfectly conducting. Furthermore, the metal plane is assumed to be rigid, reflecting the electrons which come into contact with it; such a boundary condition is a crude representation for a thin ion sheath, that is, one having a thickness between about one and three Debye lengths. The slot is



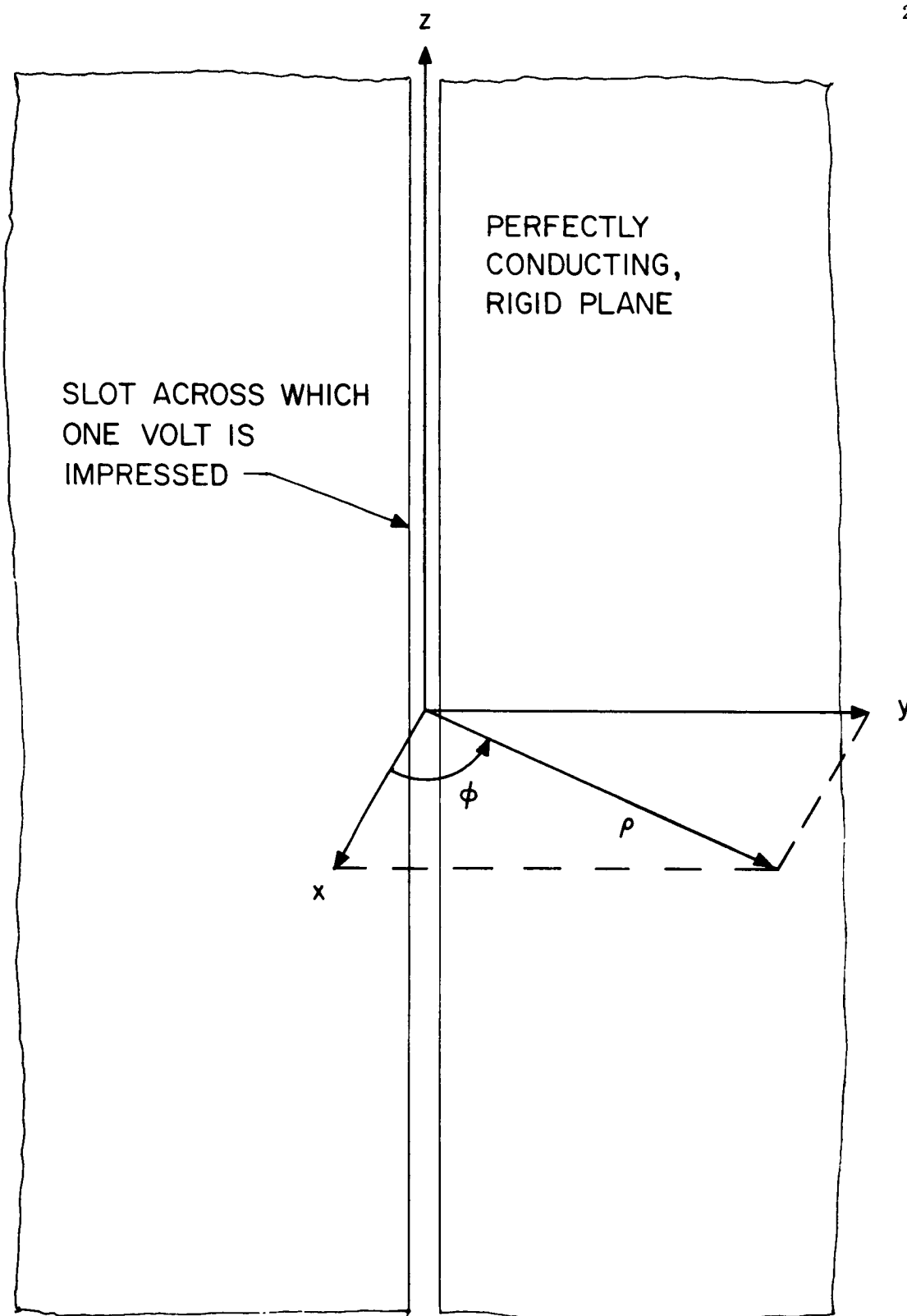


Figure 3.1 The infinitely long, narrow slot in an infinite, conducting plane.

taken to be infinitesimal in width although it is known that such an assumption will give a field solution which is incorrect in the zero temperature limit. As far as radiation fields are concerned, the infinitesimal slot is an adequate representation for a slot which is small compared to a Debye length.

The compressible plasma theory has been widely used in recent years, especially following the fundamental papers of Cohen (1961, 1962). A partial bibliography may be found in the recent paper by Balmain (1965) which also reviews the basic equations. The usual treatment involves the separation of all field quantities into two modes, the electroacoustic or "p" mode and the electromagnetic or "e" mode. The electroacoustic mode involves  $p$ ,  $\bar{E}_p$  and  $\bar{v}_p$  which are the pressure, electric field strength and velocity, respectively. The electromagnetic mode involves  $\bar{H}$ ,  $\bar{E}_e$  and  $\bar{v}_e$  which are the magnetic field strength, the electric field strength and the velocity. The total fields may be expressed as

$$\bar{E} = \bar{E}_p + \bar{E}_e \quad (1)$$

$$\bar{v} = \bar{v}_p + \bar{v}_e \quad (2)$$

In problems which concern infinite slots, it is known that  $\bar{H}$  is parallel to the slot ( $H_x = H_y = 0$ ). Thus under source-free conditions and with  $z$  derivatives zero, the basic equations reduce to

$$\left( \frac{\partial^2}{\partial x^2} + \frac{\partial^2}{\partial y^2} + k_p^2 \right) p = 0, \quad k_p^2 = \frac{\omega_m^2}{3kT} (U - X) \quad (3)$$

$$\bar{E}_p = \frac{1 - K_o}{Ne K_o} \left( \hat{x} \frac{\partial p}{\partial x} + \hat{y} \frac{\partial p}{\partial y} \right) \quad (4)$$

$$\bar{v}_p = \frac{j}{\omega u K_o Nm} \left( \hat{x} \frac{\partial p}{\partial x} + \hat{y} \frac{\partial p}{\partial y} \right) \quad (5)$$

$$\left( \frac{\partial^2}{\partial x^2} + \frac{\partial^2}{\partial y^2} + k_e^2 \right) H_z = 0, \quad k_e^2 = \omega^2 \mu_o \epsilon_o \left( \frac{U - X}{U} \right) \quad (6)$$

$$\bar{E}_e = \frac{-j}{\omega \epsilon_o K_o} \left( \hat{x} \frac{\partial H_z}{\partial y} - \hat{y} \frac{\partial H_z}{\partial x} \right) \quad (7)$$

$$\bar{v}_e = \frac{e}{\omega^2 \mu_o \epsilon_o K_o} \left( \hat{x} \frac{\partial H_z}{\partial y} - \hat{y} \frac{\partial H_z}{\partial x} \right) \quad (8)$$

The nomenclature is the same as used in Chapter 1.

The above equations will be solved with the assistance of the Fourier transforms given by

$$\tilde{f}(\gamma) = \frac{1}{2\pi} \int_{-\infty}^{\infty} f(y) e^{+j\gamma y} dy \quad (9)$$

$$f(y) = \int_{-\infty}^{\infty} \tilde{f}(\gamma) e^{-j\gamma y} d\gamma \quad (10)$$

After application of the Fourier transforms, equations (3) through (8) become

$$\left( \frac{\partial^2}{\partial x^2} + \beta_p^2 \right) \tilde{p} = 0, \quad \beta_p^2 = k_p^2 - \gamma^2, \quad (11)$$

$$\tilde{E}_p = \frac{-j(1 - K_0)}{Ne K_0} (\hat{x} \beta_p + \hat{y} \gamma) \tilde{p}, \quad (12)$$

$$\tilde{v}_p = \frac{1}{\omega U K_0 m N} (\hat{x} \beta_p + \hat{y} \gamma) \tilde{p}, \quad (13)$$

$$\left(\frac{\partial^2}{\partial x^2} + \beta_e^2\right) \tilde{H}_z = 0, \quad \beta_e^2 = k_e^2 - \gamma^2, \quad (14)$$

$$\tilde{E}_e = \frac{-1}{\omega \epsilon_0 K_0} (\hat{x} \gamma - \hat{y} \beta_e) \tilde{H}_z \quad (15)$$

$$\tilde{v}_e = \frac{-je}{\omega^2 U m \epsilon_0 K_0} (\hat{x} \gamma - \hat{y} \beta_e) \tilde{H}_z. \quad (16)$$

Differential equations (11) and (14) have exponential solutions and these solutions must decay with increasing distance from the slot. The solutions may be expressed as follows:

$$\tilde{p} = A e^{-j\beta_p x} \quad (17)$$

$$\tilde{H}_z = B e^{-j\beta_e x} \quad (18)$$

in which A and B are arbitrary "constants" (functions of the transform variable  $\gamma$ ). Under lossy conditions (when collisions are present) and for positive values of  $x$ , the decaying field condition requires that  $\beta_p$  and  $\beta_e$  have negative imaginary parts. Thus  $\beta_p$  and  $\beta_e$  may be determined uniquely for use in solutions (17) and (18). In the collisionless limit,

$$\begin{aligned}
\beta_p &= \sqrt{k_p^2 - \gamma^2} \text{ for } \gamma^2 \leq k_p^2 \\
\beta_p &= -j\sqrt{\gamma^2 - k_p^2} \text{ for } \gamma^2 \geq k_p^2
\end{aligned} \tag{19}$$

$$\begin{aligned}
\beta_e &= \sqrt{k_e^2 - \gamma^2} \text{ for } \gamma^2 \leq k_e^2 \\
\beta_e &= -j\sqrt{\gamma^2 - k_e^2} \text{ for } \gamma^2 \geq k_e^2
\end{aligned} \tag{20}$$

in which  $\sqrt{\phantom{x}}$  denotes the positive square root. It may be shown that, for this problem, the decaying field condition gives rise to fields with outward phase progression.

Having determined the functional form of the solution, it is necessary now to state the boundary conditions. Application of one volt across the infinitesimal gap requires that at  $x = 0$

$$E_y = E_{p_y} + E_{e_y} = \delta(y) \tag{21}$$

or, after transformation

$$\tilde{E}_y = \tilde{E}_{p_y} + \tilde{E}_{e_y} = \frac{1}{2\pi} . \tag{22}$$

The rigidity of the boundary demands that at  $x = 0$

$$v_x = v_{p_x} + v_{e_x} = 0 \tag{23}$$

or after transformation,

$$\tilde{v}_x = \tilde{v}_{p_x} + \tilde{v}_{e_x} = 0 \quad (24)$$

Equations (22) and (24) become, respectively,

$$\frac{\beta}{\omega U m N K_o} A - j \frac{e \gamma}{\omega^2 U m \epsilon_o K_o} B = 0 \quad (25)$$

$$-j \frac{(1 - K_o) \gamma}{N e K_o} A + \frac{\beta_e}{\omega \epsilon_o K_o} B = \frac{1}{2\pi} \quad (26)$$

Solution of (25) and (26) yields

$$A = \frac{1}{2\pi} \frac{j N e K_o \gamma}{(1 - K_o) \gamma^2 + \beta_e \beta_p} \quad (27)$$

$$B = \frac{1}{2\pi} \frac{\omega \epsilon_o K_o \beta_p}{(1 - K_o) \gamma^2 + \beta_e \beta_p} \quad (28)$$

from which the complete transformed solution may be obtained through (17), (18), (12), (13), (15) and (16).

The inverse Fourier transformation permits expression of the pressure and magnetic field strength in integral form.

$$p = j \frac{N e K_o}{2\pi} \int_{-\infty}^{\infty} \frac{-j(\beta_p x + \gamma y)}{D} e^{\gamma y} d\gamma \quad (29)$$

$$H_z = \frac{\omega \epsilon_0 K_0}{2\pi} \int_{-\infty}^{\infty} \frac{\beta_p e^{-j(\beta_e x + \gamma y)}}{D} d\gamma \quad (30)$$

in which  $D = (1 - K_0) \gamma^2 + \beta_e \beta_p$ .

The remaining field quantities may be expressed similarly as integrals or they may be derived using (4), (5), (7) and (8). In integral form they are

$$\bar{v}_p = j \frac{e}{2\pi\omega U m} \int_{-\infty}^{\infty} \frac{(\hat{x}\beta_p + \hat{y}\gamma)\gamma}{D} e^{-j(\beta_p x + \gamma y)} d\gamma \quad (31)$$

$$\bar{E}_p = \frac{1 - K_0}{2\pi} \int_{-\infty}^{\infty} \frac{(\hat{x}\beta_p + \hat{y}\gamma)\gamma}{D} e^{-j(\beta_p x + \gamma y)} d\gamma \quad (32)$$

$$\bar{v}_e = -j \frac{e}{2\pi\omega U m} \int_{-\infty}^{\infty} \frac{(\hat{x}\gamma - \hat{y}\beta_e)\beta_p}{D} e^{-j(\beta_e x + \gamma y)} d\gamma \quad (33)$$

$$\bar{E}_e = \frac{-1}{2\pi} \int_{-\infty}^{\infty} \frac{(\hat{x}\gamma - \hat{y}\beta_e)\beta_p}{D} e^{-j(\beta_e x + \gamma y)} d\gamma \quad (34)$$

In the above form, the integrations are difficult to work with. They may be made more tractable by rationalizing the denominator, that is by multiplying numerator and denominator by  $(1 - K_0) \gamma^2 - \beta_e \beta_p$ . The rationalized denominator is given by

$$\begin{aligned} (1 - K_0)^2 \gamma^4 - \beta_e^2 \beta_p^2 &= \left[ \left( \frac{\chi}{u} \right)^2 - 1 \right] \gamma^4 + (k_e^2 + k_p^2) \gamma^2 - k_e^2 k_p^2 \\ &= - \left[ M \gamma^4 - (k_e^2 + k_p^2) \gamma^2 + k_e^2 k_p^2 \right] \end{aligned} \quad (35)$$

in which  $M = 1 - \left( \frac{\chi}{u} \right)^2$ .

At this point it is convenient to regard  $\gamma$  as a complex variable; the integrations in (29) to (34) are thus along the real axis in the  $\gamma$  plane. The integrand contains a number of critical points lying in the  $\gamma$  plane. These are the branch points at  $\gamma = \pm k_e$  and  $\gamma = \pm k_p$  together with the poles (zeros of the rationalized denominator) at  $\gamma = \pm \gamma_s$  and  $\gamma = \pm \gamma_o$ . The quantities  $\gamma_s$  and  $\gamma_o$  are given by

$$\left. \begin{array}{l} \gamma_s^2 \\ \gamma_o^2 \end{array} \right\} = \frac{k_e^2 + k_p^2}{2M} \left[ 1 \pm \sqrt{1 - \frac{4M k_e^2 k_p^2}{(k_e^2 + k_p^2)^2}} \right] \quad (36)$$

In most cases of interest  $k_p \gg k_e$ , the ratio of these two quantities being of the order of  $10^3$ . This permits the roots in (36) to be expressed in series form as follows:

$$\gamma_s^2 = \frac{k_p^2}{M} + \dots \quad (37)$$

$$\gamma_o^2 = k_e^2 + \frac{(M-1) k_e^4}{k_p^2} + \dots \quad (38)$$

Note that the pole location  $\gamma_o$  is very nearly coincident with the branch point at  $k_e$ .

Due to the presence of square roots, the integrands are multiple-valued. Since square roots arise in two quantities  $\beta_p$  and  $\beta_e$ , four combinations of roots may be chosen. Thus all the possible values of any integrand correspond to all the points on a four-sheeted Riemann surface in the complex  $\gamma$  plane. One of these sheets is specified by the decaying field criterion already discussed and this sheet will be referred to as the "proper" sheet. An



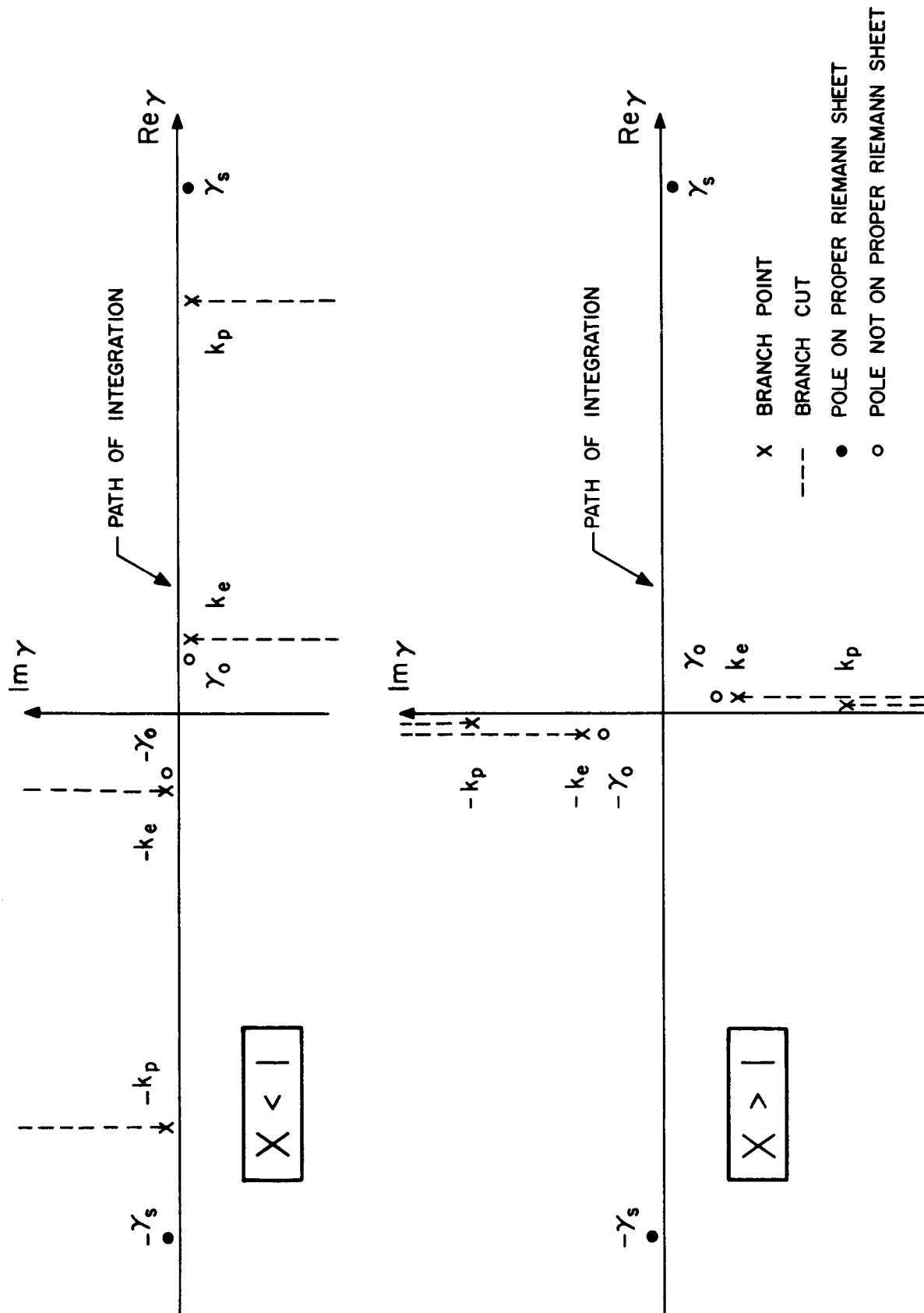


Figure 3.2 Integration Contours.

examination of the poles reveals that  $\pm \gamma_s$  lie on the proper sheet but  $\pm \gamma_o$  do not. The pole and branch point locations are shown in Figure 3.2 for frequencies above and below the plasma frequency. Figure 3.2 shows that the poles at  $\pm \gamma_s$  will have a strong influence at all frequencies. Although the poles at  $\pm \gamma_o$  are not on the proper sheet, they are nevertheless very close to the path of integration because of their proximity to the branch points at  $\pm k_e$ ; consequently these poles may influence the field solution appreciably at frequencies above plasma frequency.

### 3.3 Far Field Solution

The far field evaluation of the integrals is carried out by the method of steepest descents. Once a steepest descent path has been selected the integral along this path can be related to the original integral by the Cauchy integral theorem. Thus the far field solution in general consists of the asymptotic approximation to the steepest descent integral plus the residue at any pole lying between the steepest descent path and the real axis in the  $\gamma$  plane. The pole contribution consists of a surface wave as found by Seshadri (1964); the steepest descent integrals contribute space waves radiated outward from the slot. In this report the electromagnetic and electroacoustic space waves will be examined and compared with the surface wave. The evaluation of the field integrals will not be carried out in detail here since similar integrals have been evaluated with great care by Langelier (1964).

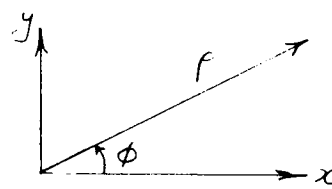
#### 3.3.1 The Space Waves

In order to simplify the calculations, the space wave derivation will be carried out under lossless conditions ( $U = 1$ ). Furthermore the space

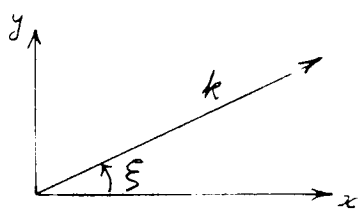
waves propagate only at frequencies greater than the plasma frequency so that  $X < 1$ . Under these conditions the quantities  $k_e$  and  $k_p$  are positive real numbers. Integrals (29) to (34) all have the form

$$f(y) = \int_{-\infty}^{\infty} G(\gamma) e^{-j(\beta x + \gamma y)} d\gamma \quad (39)$$

in which  $\beta^2 = k^2 - \gamma^2$  and  $k$  is a positive real number. It is convenient to transform into cylindrical coordinates at this point. The transformation is given below:



$x = \rho \cos \phi$   
 $y = \rho \sin \phi$



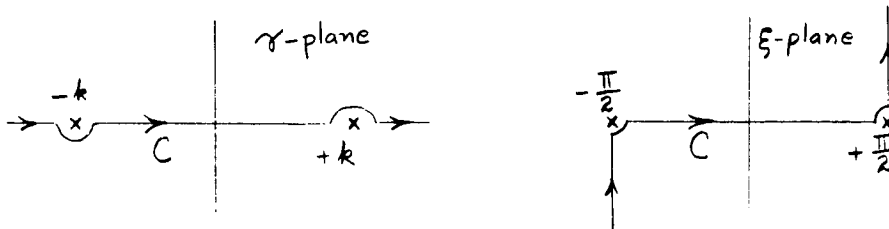
$\beta = k \cos \xi$   
 $\gamma = k \sin \xi$

(40)

This transformation puts (39) into the form

$$f(y) = k \int_C G(k \sin \xi) e^{-jk\rho \cos(\xi-\phi)} \cos \xi d\xi \quad (41)$$

for which the contour  $C$  in the  $\xi$  plane is sketched below:



At this point the method of steepest descent or the method of stationary phase may be used; both methods have been summarized recently by Jones (1964). The saddle point (or point of stationary phase) is at  $\xi = \phi$  and asymptotic evaluation of (41) along the steepest descent path yields, for large values of  $\rho$ ,

$$f(y) = k \cos \phi \sqrt{\frac{2\pi}{k\rho}} G(k \sin \phi) e^{-jk\rho + j\frac{\pi}{4}} \quad (42)$$

The above formula may be used to obtain far field expressions for the electromagnetic or "e" mode by setting  $k = k_e$  and for the electroacoustic or "p" mode by setting  $k = k_p$ .

For the electroacoustic mode the pressure integral (29) becomes

$$p = j \frac{Ne k_o}{2\pi} I(\rho, \phi) \quad (43)$$

in which

$$I(\rho, \phi) = \frac{k_p^2 \sin \phi \cos \phi}{(1 - K_o) k_p^2 \sin^2 \phi + \sqrt{k_e^2 - k_p^2 \sin^2 \phi} k_p \cos \phi} \sqrt{\frac{2\pi}{k_p \rho}} e^{-jk_p \rho + j\frac{\pi}{4}}$$

At the saddle point, the direction of the velocity vector  $\bar{v}_p$  as given by (31) is

$$\begin{aligned} \hat{x}_p \beta_p + \hat{y}_p \gamma &= (\hat{x} \cos \phi + \hat{y} \sin \phi) k_p \\ &= \hat{\rho} k_p \end{aligned} \quad (44)$$

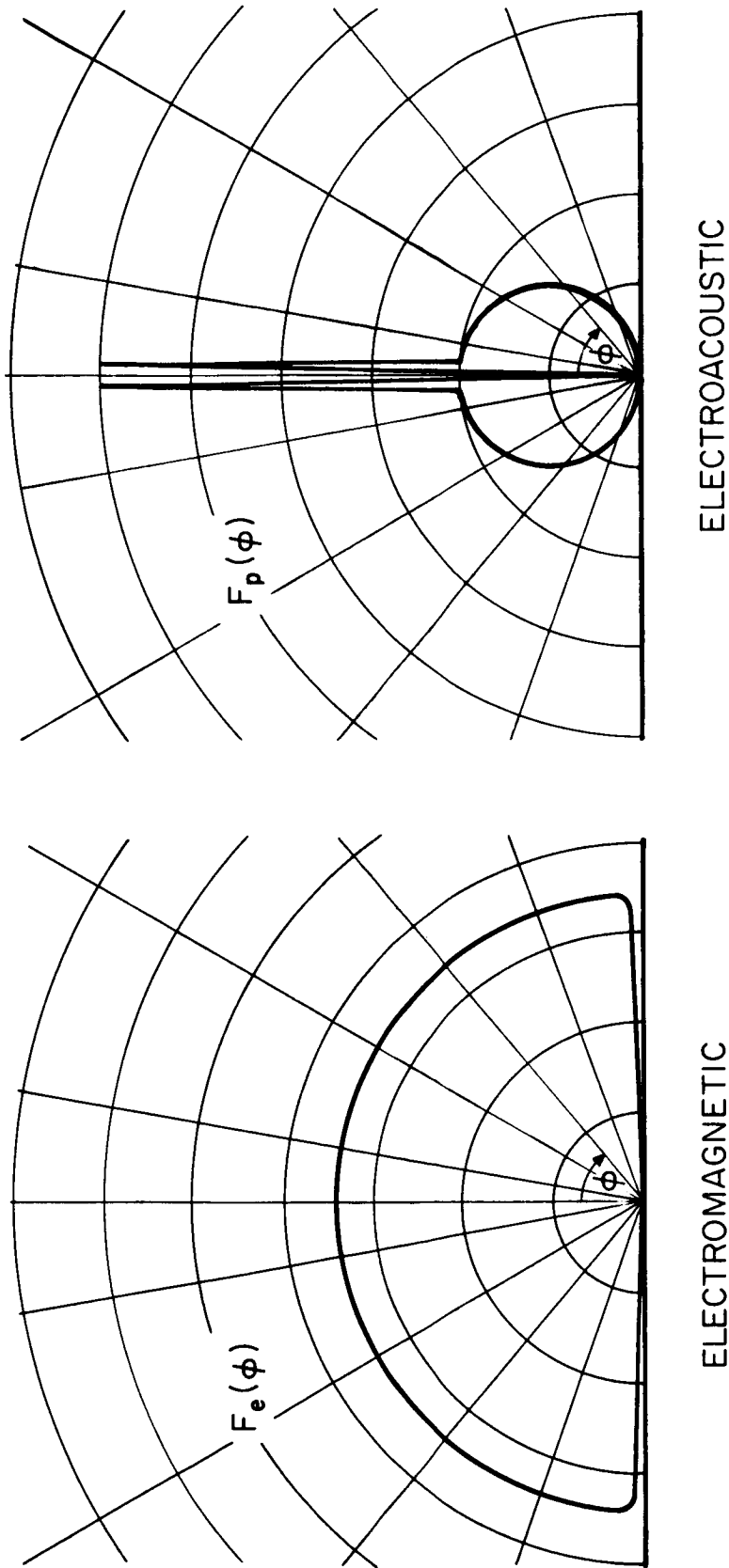


Figure 3.3 Space wave radiation patterns .

and thus the "p" mode velocity is entirely radial. Consequently, the velocity may be expressed as

$$v_{p\rho} = j \frac{e k_p}{2\pi\omega m} I(\rho, \phi) \quad (45)$$

The "p" mode radial Poynting vector  $S_p$  may be written down using (43) and (45):

$$\begin{aligned} S_p &= \frac{1}{2} P v_{pr}^* \\ &= \frac{1}{8\pi^2} \omega \epsilon_0 X K_0 k_p I I^* \end{aligned} \quad (46)$$

The radial Poynting vector is proportional to the square of the magnitude of the quantity  $F_p(\phi)$ , given by

$$F_p(\phi) = \frac{\sin \phi \cos \phi}{X \sin^2 \phi + \sqrt{n^2 - \sin^2 \phi} \cos \phi} \quad (47)$$

in which  $n = k_e/k_p \approx 10^{-3}$ . The quantity  $F_p(\phi)$  is the radiation pattern and it is sketched approximately in Figure 3.3.

The striking feature of this radiation pattern is the presence of a pair of sharp lobes on either side of  $\phi = 0$  with a null between them. The lobes peak at  $\sin \phi = \pm n \approx \phi$  and at the peak,  $|F_p| = (Xn)^{-1}$ , a quantity which is very large compared to the rest of the radiation pattern for which  $|F_p|$  is of the order of unity. Although the lobes have a high amplitude, they are exceedingly narrow, the half-power beamwidth being approximately

$0.6 \chi^2 n^3$  radians. The ratio of power in the lobes to power in the rest of the radiation pattern is of the order of  $n^{-1}$  and thus the contribution of the lobes to the electroacoustic radiation resistance is negligible. From a purely mathematical point of view it may be observed that the lobes occur as the saddle point passes by the branch point at  $\gamma = \pm k_e$ . At these points the influence of the poles at  $\gamma = \pm \gamma_0$  is greatest and thus it is possible to conclude that the sharp sidelobes result from the influence of poles which are not on the proper Riemann sheet.

The power radiated per unit length in the electroacoustic space wave on one side of the conducting sheet ( $P_p$ ) now may be found using a modified pattern function which ignores the sharp sidelobes. This function is given by

$$F_p(\phi) = \frac{\cos \phi}{\chi \sin \phi - j \cos \phi} \quad (48)$$

Using this function, the radiated power is

$$\begin{aligned} P_p &= \int_{-\frac{\pi}{2}}^{+\frac{\pi}{2}} \operatorname{Re} \{S_p\} \rho d\phi \\ &= \frac{1}{4} \omega \epsilon_0 \chi \frac{1 - \chi}{1 + \chi} \end{aligned} \quad (49)$$

It will be noticed that  $P_p$  is independent of temperature and thus cannot vanish in the zero temperature limit. This is entirely the result of having

assumed an infinitesimal slot; the choice of a finite slot would provide the correct limiting behavior but would still give (49) as an approximation for a slot width small compared to a Debye length.

For the electromagnetic mode, the magnetic field integral (30) becomes

$$H_z = \frac{\omega \epsilon_0 K_0}{2\pi} J(\rho, \phi) \quad (50)$$

in which

$$J(\rho, \phi) = \frac{\sqrt{k_p^2 - k_e^2 \sin^2 \phi} k_e \cos \phi}{(1 - K_0) k_e^2 \sin^2 \phi + k_e \cos \phi \sqrt{k_p^2 - k_e^2 \sin^2 \phi}} \sqrt{\frac{2\pi}{k_e \rho}} e^{-jk_e \rho + j \frac{\pi}{4}}.$$

At the saddle point, the direction of the electric field strength

$\bar{E}_e$  as given by (34) is

$$\begin{aligned} \hat{x} \gamma - \hat{y} \beta_e &= (\hat{x} \sin \phi - \hat{y} \cos \phi) k_e \\ &= -\hat{\phi} k_e \end{aligned} \quad (51)$$

Thus the electric field strength may be expressed as

$$E_{e\phi} = \frac{k_e}{2\pi} J(\rho, \phi) \quad (52)$$

The radial "e" mode Poynting vector now may be written down using (50) and (52):



$$\begin{aligned}
 S_e &= \frac{1}{2} E_{e\phi} H_z^* \\
 &= \frac{\omega \epsilon_0 K_o k_e}{8\pi^2} J J^*
 \end{aligned} \tag{53}$$

The radial Poynting vector is proportional to the square of the magnitude of the quantity  $F_e(\phi)$ , given by

$$F_e(\phi) = \frac{\sqrt{1 - n^2 \sin^2 \phi} \cos \phi}{Xn \sin^2 \phi + \cos \phi \sqrt{1 - n^2 \sin^2 \phi}} \tag{54}$$

The radiation pattern  $|F_e(\phi)|$  is very nearly equal to unity for all values of  $\phi$  except very close to  $\phi = \pm \frac{\pi}{2}$ . At  $\phi = \pm \frac{\pi}{2}$ , the finite temperature of the plasma causes  $F_e$  to drop to zero as sketched approximately in Figure 3.3. This means that far from the slot the "e" mode field is zero on the conducting surface and thus there are no "e" mode currents flowing in the conductor. Since the null at  $\phi = \pm \frac{\pi}{2}$  is very narrow, it can be ignored in computing the electromagnetic power per unit length radiated on one side of the conducting plane. This power is given by

$$\begin{aligned}
 P_e &= \int_{-\frac{\pi}{2}}^{\frac{\pi}{2}} \text{Re} \{S_e\} \rho d\phi \\
 &= \frac{1}{4} \omega \epsilon_0 (1 - X) .
 \end{aligned} \tag{55}$$

### 3.3.2 The Surface Wave

As shown by Seshadri (1964), a surface wave arises from the residue of the pole at  $\gamma = \gamma_s$ . From the work of Langelier (1964) it is clear that this residue must be included in the far field computation at any point close to the conducting plane. Since the surface wave problem has already been studied by Seshadri, the treatment here will be brief.

For positive values of  $y$  it is clear from Figure 3.2 that closure of the path of integration must be in the lower half plane, encircling the pole at  $\gamma = \gamma_s$ . All the field integrals may be evaluated using the Cauchy integral theorem and the evaluation may be carried out under lossy conditions without undue complication; however, only the lossless case will be considered here. The significant field quantities are as follows (with  $M = 1 - X^2$ ):

$$P = -NeK_o \frac{X}{M} e^{-k_p M^{-1/2}(Xx + jy)} \quad (56)$$

$$v_{p_y} = -\frac{e}{\omega m} \frac{X}{M} \frac{k_p}{\sqrt{M}} e^{-k_p M^{-1/2}(Xx + jy)} \quad (57)$$

$$v_{e_y} = \frac{e}{m} \frac{X^2}{M} \frac{k_p}{\sqrt{M}} e^{-k_p M^{-1/2}(x + jy)} \quad (58)$$

$$H_z = K \frac{X^2}{M} e^{-k_p M^{-1/2}(x + jy)} \quad (59)$$

$$E_{e_x} = -\frac{k_p X^2}{M \sqrt{M}} e^{-k_p M^{-1/2}(x + jy)} \quad (60)$$

$$E_{p_x} = \frac{k_p \chi^3}{M \sqrt{M}} e^{-k_p M^{-1/2}(\chi x + jy)} \quad (61)$$

In contrast to the space waves, the surface wave does not break up into independent "p" and "e" modes. Thus the Poynting vector in the y direction for the surface wave is

$$S_s = \frac{1}{2} \left[ P_{p_y}^* + P_{e_y}^* + E_{p_x} H_z^* + E_{e_x} H_z^* \right]. \quad (62)$$

Integration of the Poynting vector over all values of x from zero to infinity gives an expression for the total power per unit length in the surface wave on one side of the conducting sheet:

$$P_s = \frac{\omega \epsilon_0}{2} \frac{\chi^2}{1 + \chi} \quad (63)$$

Attention must be drawn to the fact that the surface wave propagates at all frequencies. Furthermore, the propagation constant is of the same order of magnitude as the "p" mode space wave propagation constant. Thus the surface wave has a very slow phase velocity and a very short wavelength. The inclusion of collisions reveals that the surface wave and both the space waves have roughly the same attenuation per wavelength but because of their very short wavelength, the surface wave and the "p" mode space wave have an attenuation per unit length which is very great compared to that of an electromagnetic space wave. For example, at  $\chi = 4$ ,  $T = 300^\circ K$  and  $Z = .02$ , the surface wave is attenuated by a factor of  $\frac{1}{e}$  in a hundredth of a free space wavelength.

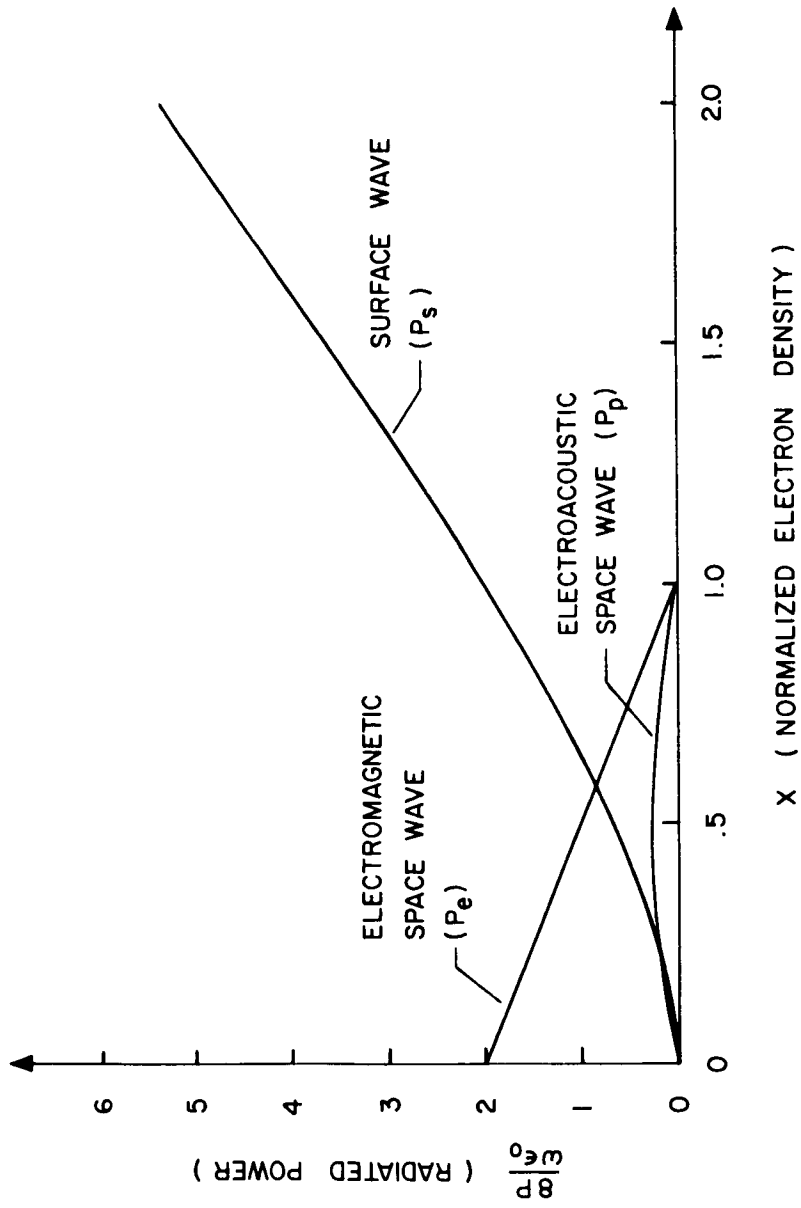


Figure 3.4 A comparison of power radiated in the three modes.

### 3.4 Discussion of the Results

The three expressions for radiated power are (49), (55) and (63) which are plotted as functions of  $X$  in Figure 3.4. For all values of  $X$  above 0.6, the surface wave provides the principal mechanism for carrying power away from the slot. Thus for the idealized problem discussed here, the surface wave would contribute very markedly to the input conductance of the slot.

Since practical antennas are necessarily finite in size, the surface wave would be reflected from the ends of the antenna structure and thus could not contribute to a net power outflow, at least in the lossless case. However, with collisional losses included, in most cases of interest the surface wave would be greatly attenuated before reaching the end of the antenna. Thus the surface wave power radiated on an infinite structure can be used to estimate the surface wave power lost on a finite structure.

The "p" mode space wave carries little power compared to the other two modes. This wave does have the very interesting feature of a pair of very sharp sidelobes, however. Although these sidelobes make a negligible contribution to the radiation conductance, it may still be possible to detect them experimentally by a very careful field measurement.

The rigid boundary condition applied at the metal surface is a very crude representation for the ion sheath, an electron-depleted region which usually is several Debye lengths thick. The surface wave analysis as presented here is valid only when the sheath thickness is small compared to the penetration height of the surface waves above the conducting plane. From equations (56) to (61) it is clear that there are two penetration

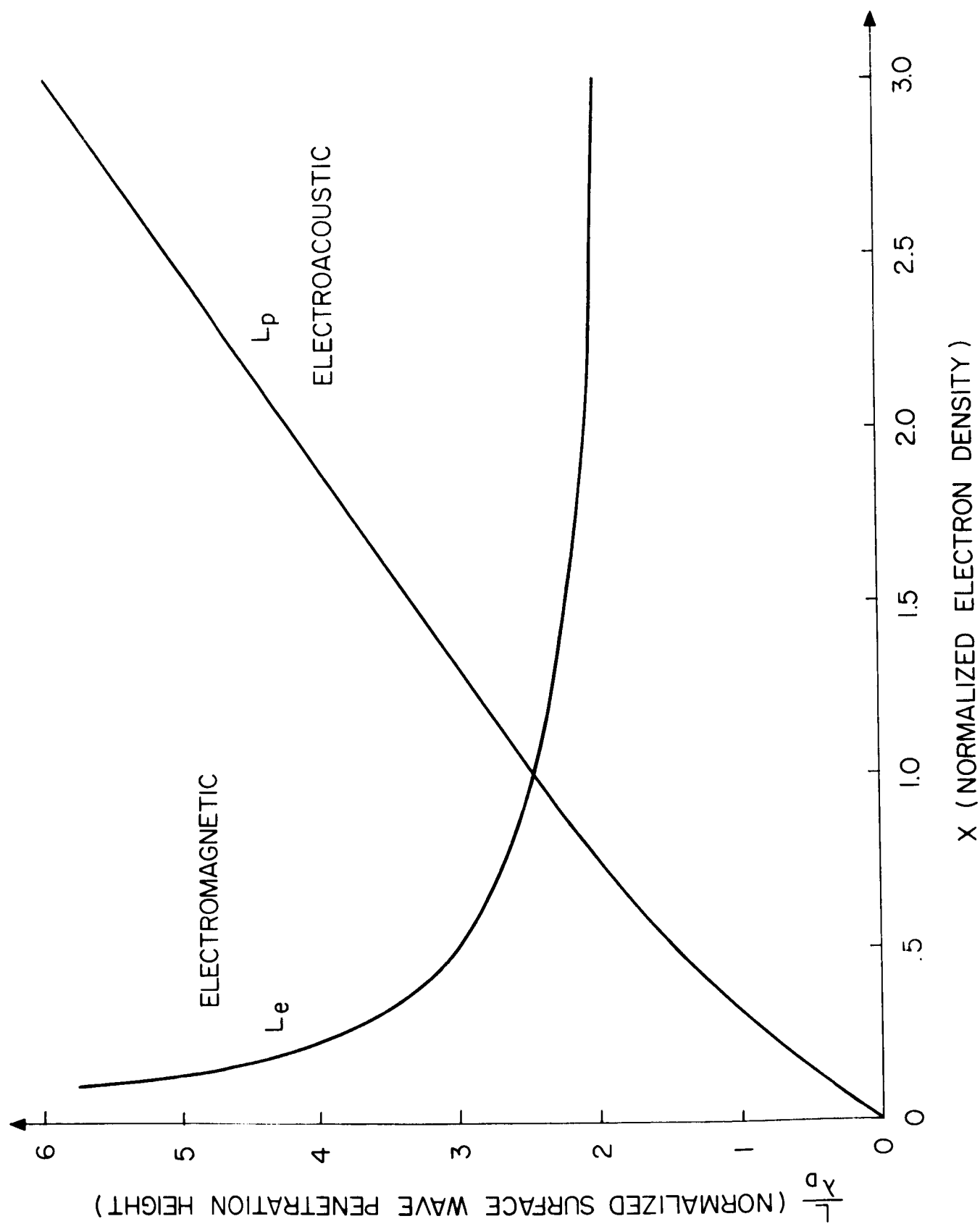


Figure 3.5 Surface wave penetration heights.

heights,  $L_e$  (associated with the electromagnetic part of the field) and  $L_p$  (associated with the electroacoustic part). These penetration heights are plotted in Figure 3.5 from which it is clear that the surface wave analysis tends to be valid only in the vicinity of  $X = 1$  and then only for sheath thicknesses between one and two Debye lengths (for sheath thicknesses less than  $\lambda_D$ , surface absorption would render the analysis invalid). For a sheath thickness of  $2 \lambda_D$ , the range of validity would be  $.75 < X < 3.0$ .

The results of the analysis lead to some suggestions regarding the current distribution on an antenna immersed in a plasma. As already observed, the surface wave with its very short wavelength can be strongly excited and since this wave has a tangential magnetic field, a surface current must be associated with it. On the other hand, the electromagnetic space wave amplitude goes to zero close to the conducting plane. These observations lead to the suggestion that antenna current distributions could have an appreciable surface wave (short wavelength) component.

#### 4. ION COLLECTION BY A SPHERICAL DC PROBE AT HIGH PRESSURES

##### 4.1 Introduction

This report is concerned with the direct measurement of positive ion densities in the ionosphere within the altitude range of 50 to 90 km. The measurement technique to be studied involves a negatively biased spherical probe projecting from the side of a rocket. If the magnitude of the probe voltage is high enough with respect to the rocket body, only positively charged ions are attracted to the probe; the electrons and negative ions are repelled and do not contribute directly to the probe current.

The probe current is a complicated function of the ion species, density and temperature and, furthermore, the current is influenced by such factors as rocket velocity and photoemission. The present objective is to deduce the ion density from the measured probe current using theory applicable to a stationary probe. Such a procedure requires an estimate of ion species and temperature together with the minimization of photoemission and rocket velocity effects. The latter effects are difficult to deal with, but it is expected that a high probe voltage will reduce velocity effects by giving the ions terminal velocities appreciably greater than the rocket velocity. Photoemission, of course, depends on the presence of sunlight and thus it should have no effect on the pre-sunrise and post-sunset rocket firings being carried out in the IQSY program.

In the altitude range of interest, the air pressure is high enough to cause the ions to make many collisions with molecules while being attracted to the probe. Under these conditions, the drift velocity of  $v$  of the ions is a function of the electric field strength  $E$ . In the noble gases  $v \propto E$  if  $E$  is small and  $v \propto E^{1/2}$  if  $E$  is large; the transition is in the vicinity of



$v \approx 10^5$  cm/sec and  $E/P_0 = 50$  volt/cm-mm H<sub>g</sub> where  $P_0$  is the reduced pressure given by  $\frac{273 P}{T}$ . In the atmospheric gases, the high-field proportionality is different, being  $v \propto E^{0.6}$  for  $N_2^+$  ions in  $N_2$  (McDaniel, 1964). The proportionalities discussed above all have the form

$$v = \alpha E^\beta$$

$$= \eta \left( \frac{E}{P_0} \right)^\beta$$

in which  $\alpha = \eta/P_0^\beta$ . Since  $\beta$  may lie anywhere between 0.5 and 1.0, it is clearly advisable for theoretical studies to be carried out for an arbitrary value of  $\beta$ .

An ion-collection theory for cylindrical probes with  $\beta = 1$  has been derived by Schulz and Brown (1955) and verified experimentally in the laboratory by comparison with microwave cavity measurements. A similar probe theory with  $\beta = 1/2$  has been derived by Aono, et al. (1962) and used to deduce ion densities in the ionosphere. These theories take space charge into account and postulate a well-defined boundary separating the ambient plasma and the ion sheath. The ion sheath is assumed to contain only ions (positive ones) and these ions enter the sheath region with a current density taken to be the same as the random ion current density in an infinite uniform plasma. Such a theoretical approach leaves much to be desired, especially because it ignores diffusion and postulates a well-defined sheath-plasma interface. On the other hand, this approach does yield a relatively simple solution, some aspects of which have been verified experimentally. Consequently, the assumptions outlined above will be used in this report, but the value of  $\beta$  will be left arbitrary.

#### 4.2 A General Spherical Probe Theory

The relationship between ion drift velocity and electric field discussed in the introduction may be expressed as a relation between inward current density  $J$  and potential  $V$ :

$$J = ne \propto \left(\frac{dV}{dr}\right)^{\beta} \quad (1)$$

Here  $e$  is the ionic charge magnitude (assuming singly charged ions) and  $n$  is the ion density which is a function of the radius  $r$  within the ion sheath. It is assumed that the total current  $i$  is constant in the sheath; thus the current density is given by

$$J = \frac{i}{4\pi r^2} \quad (2)$$

The charge density now may be expressed as

$$\rho = ne = \frac{i}{4\pi r^2 \propto \left(\frac{dV}{dr}\right)^{\beta}} \quad (3)$$

The basic quantities defined above are related by Poisson's equation which expresses mathematically the interaction between the ion space charge and the ion drift velocity due to a potential gradient. Poisson's equation in rationalized MKS units may be expressed in spherical coordinates and manipulated as follows:

$$\nabla^2 V = - \frac{\rho}{\epsilon} \quad (4)$$

$$\frac{1}{r^2} \frac{d}{dr} \left( r^2 \frac{dV}{dr} \right) = - \frac{i}{4\pi\epsilon r^2 \alpha \left( \frac{dV}{dr} \right)^\beta} \quad (5)$$

$$r^2 \left( \frac{dV}{dr} \right)^\beta \frac{d^2 V}{dr^2} + 2r \left( \frac{dV}{dr} \right)^\beta \frac{dV}{dr} = - \frac{i}{4\pi\epsilon\alpha} \quad (6)$$

At this point it should be noted that

$$\frac{d}{dr} \left[ \left( \frac{dV}{dr} \right)^{1+\beta} \right] = (1+\beta) \left( \frac{dV}{dr} \right)^\beta \frac{d^2 V}{dr^2} . \quad (7)$$

Substitution into Poisson's equation yields

$$\frac{r^2}{1+\beta} \frac{d}{dr} \left[ \left( \frac{dV}{dr} \right)^{1+\beta} \right] + 2r \left( \frac{dV}{dr} \right)^{1+\beta} = \frac{-i}{4\pi\epsilon\alpha} \quad (8)$$

It is convenient to introduce the definition

$$W = \left( \frac{dV}{dr} \right)^{1+\beta} \quad (9)$$

which permits Poisson's equation to be expressed as

$$r^2 \frac{dW}{dr} + 2(1+\beta) r W = - \frac{(1+\beta) i}{4\pi\epsilon\alpha} \quad (10)$$

The next step is to express the left hand side of the above equation as an exact differential. Note that, in general,

$$\begin{aligned} \frac{d}{dr} (r^m W) &= r^m \frac{dW}{dr} + m r^{m-1} W \\ &= r^q \left[ r^{m-q} \frac{dW}{dr} + m r^{m-q-1} W \right] \end{aligned} \quad (11)$$

Matching the quantity in square brackets with the left hand side of (10), we find that

$$m = 2(1 + \beta), \quad m - q - 1 = 1, \quad q = m - 2 = 2\beta. \quad (12)$$

Consequently (10) becomes

$$\frac{d}{dr} \left[ r^{2(1+\beta)} W \right] = - \frac{(1+\beta) i}{4 \pi \epsilon \alpha} r^{2\beta}. \quad (13)$$

Having been simplified as much as possible, the differential equation is now ready for integration which gives

$$r^{2(1+\beta)} W = - \frac{(1+\beta) i}{(1+2\beta) 4 \pi \epsilon \alpha} (r^{1+2\beta} + C) \quad (14)$$

The first boundary condition is that the potential gradient be zero at the sheath edge. That is,

$$W = 0 \text{ at } r = a \quad (15)$$

which permits evaluation of the arbitrary constant.

$$C = - a^{1 + 2\beta}. \quad (16)$$

Equation (14) now may be written

$$W = \frac{i (1 + \beta)}{4\pi\epsilon\alpha (1 + 2\beta)} \cdot \frac{1}{r} \cdot \left[ \left(\frac{a}{r}\right)^{1 + 2\beta} - 1 \right]. \quad (17)$$

If the radial coordinate is normalized by writing  $r = ax$ , (17) becomes

$$\frac{dV}{dx} = B \frac{(1 - x^{1 + 2\beta})^{\frac{1}{1 + \beta}}}{x^2} \quad (18)$$

$$\text{in which } B = \left[ \frac{i a^\beta (1 + \beta)}{4\pi\epsilon\alpha (1 + 2\beta)} \right] \frac{1}{1 + \beta}.$$

Integration with respect to  $x$  and application of the second boundary condition

$$V = 0 \text{ at } x = 1 \quad (19)$$

yields an integral expression for the potential at any point  $x$  within the sheath.

$$V = - B \int_x^1 \frac{(1 - u^{1 + 2\beta})^{\frac{1}{1 + \beta}}}{u^2} du \quad (20)$$

Let the conditions at the probe surface be given by  $V = - V_0$ ,  $x = x_0$ ,

$r = r_0$ . Here  $V_0$  may be interpreted as the magnitude of the negative voltage applied to the probe (with respect to the plasma). Thus (20) may be expressed as

$$V_0 = B \int_{x_0}^1 \frac{(1 - u^{1+2\beta})^{\frac{1}{1+\beta}}}{u^2} du. \quad (21)$$

This integral may be evaluated exactly only for certain values of  $\beta$  and for some of these the expression contains elliptic integrals. However, inspection of (21) reveals that for small values  $x_0$ , the value of the integral will be dominated by the  $u^{-2}$  factor in the integrand. A small  $x_0$  means that the probe radius  $r_0$  is small compared to the sheath radius "a". Either an integration of  $u^{-2}$  or integration of (21) by parts will separate out the dominant term for small  $x_0$ . The latter procedure yields

$$\frac{V_0}{B} = \frac{(1 - x_0^{1+2\beta})^{\frac{1}{1+\beta}}}{x_0} - \frac{1+2\beta}{1+\beta} \int_{x_0}^1 \frac{u^{2\beta-1}}{(1 - u^{1+2\beta})^{\frac{\beta}{1+\beta}}} du \quad (22)$$

As  $x_0 \rightarrow 0$  the integral remains finite for  $1/2 \leq \beta \leq 1$ . Thus in the limit, (22) approaches

$$V_0 = \frac{B}{x_0} \quad (23)$$

Equations (21) and (23) do not constitute voltage-current relations because they contain a third unknown, the sheath radius  $a$ . This problem

can be eliminated by assuming that the current density at the sheath edge is equal to the random ion current density  $J_r$  in the plasma. Thus

$$\frac{i}{4\pi a^2} = J_r = Ne \sqrt{\frac{kT}{2\pi M}} \quad (24)$$

in which  $N$ ,  $M$  and  $T$  are respectively the number density, mass and temperature of the ions. Substitution of (24) into (23) yields the voltage-current relation

$$V_o = \frac{1}{r_o (4\pi J_r)^{\frac{1}{2}} \cdot \frac{1+2\beta}{1+\beta}} \left[ \frac{1+\beta}{4\pi e \alpha (1+2\beta)} \right]^{\frac{1}{1+\beta}} \frac{1}{i^{\frac{1}{2}}} \cdot \frac{3+2\beta}{1+\beta} \quad (25)$$

It is worth noting that the shape of the voltage-current curve depends on  $\beta$  alone.

A common ionospheric probing technique involves deduction of the ion density from the probe current for a fixed voltage. If the field-velocity dependence is expressed as

$$v = \eta \left( \frac{E}{P_o} \right)^\beta, \quad (26)$$

then

$$\alpha = \eta P_o^{-\beta} \quad (27)$$

where  $P_o$  is the "reduced pressure"  $273 P/T$ ,  $P$  being the measured gas pressure and  $T$  the temperature in  $^{\circ}\text{K}$ . Making use of (27) one may express

the ion density as

$$N = \frac{P_o^{\frac{2\beta}{1+2\beta}}}{4\pi e \sqrt{\frac{kT}{2\pi M}}} \left[ \frac{(1+\beta)}{4\pi e \eta (1+2\beta) (r_o V_o)^{1+\beta}} \right]^{\frac{2}{1+2\beta}} i^{\frac{3+2\beta}{1+2\beta}}. \quad (28)$$

The quantities  $\beta$  and  $\eta$  may be deduced from laboratory experiments (Brown, 1959; McDaniel, 1964). The potential  $V_o$  is the probe-to-plasma potential; it is given by the applied voltage reduced by the estimated potential difference across the ion sheath surrounding the reference electrode. The quantities  $T$ ,  $M$  and  $P_o$  must also be estimated in order to relate the ion density to the measured current.

### 4.3 Measurements in the Ionosphere

#### 4.3.1 Collisionless Theory

The theory developed so far has been concerned with ion motion dominated by collisions. In other words, the ambient gas pressure was considered to be high enough so that an ion would undergo many collisions while traversing the sheath region around the probe. On the other hand, for very low pressures there exists a body of spherical probe theory which has been discussed at length by many authors, including Boggess (1959) whose work will be summarized here. If the sheath is very large ( $a/r_o \gg 1$ ) and if a large negative potential ( $-V_o$ ) is applied to the probe, then kinetic theory gives the probe current as

$$i = A J_r \left( 1 + \frac{eV_o}{kT} \right) \quad (29)$$



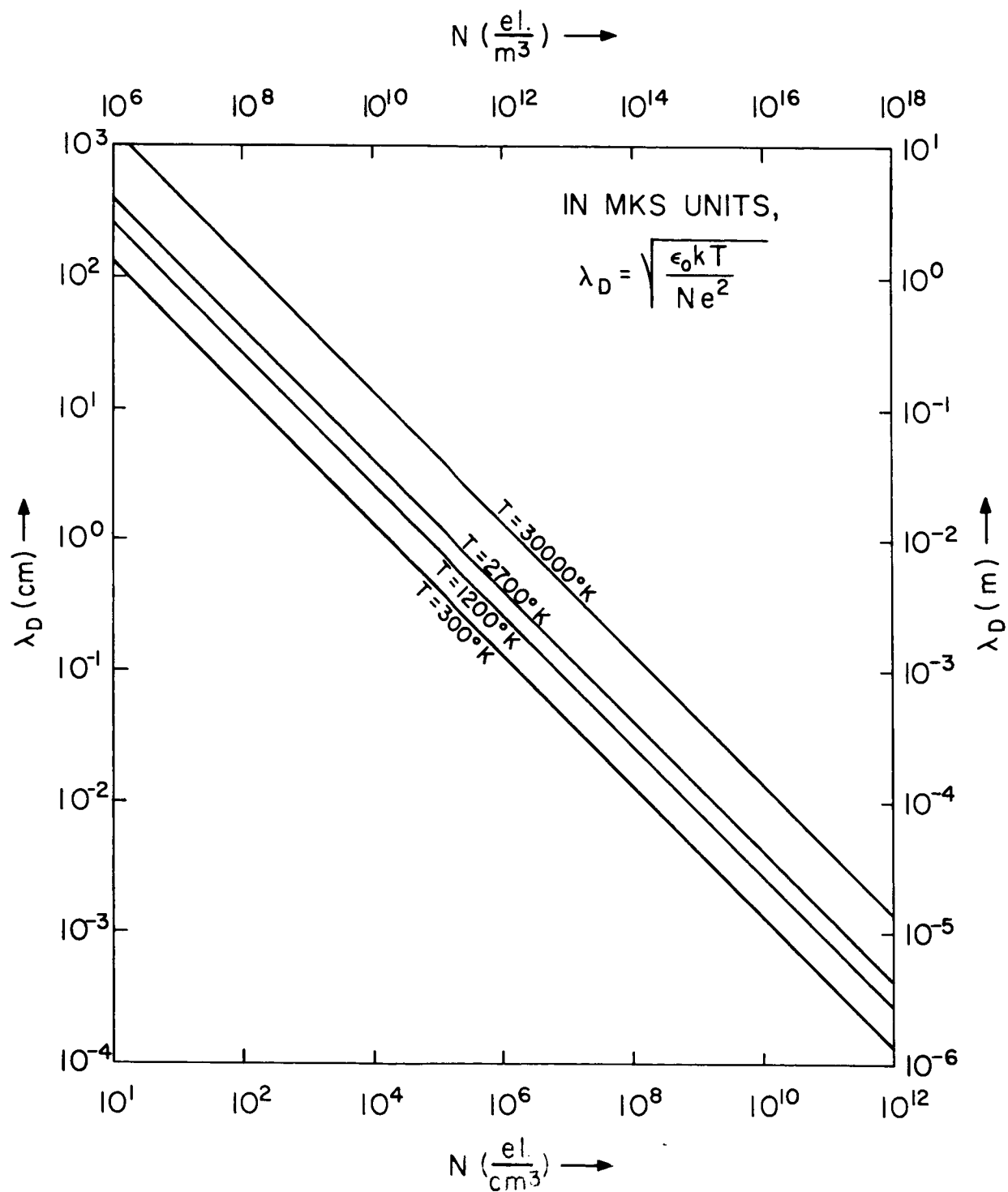


Figure 4.1 The Debye-Hückel shielding length.

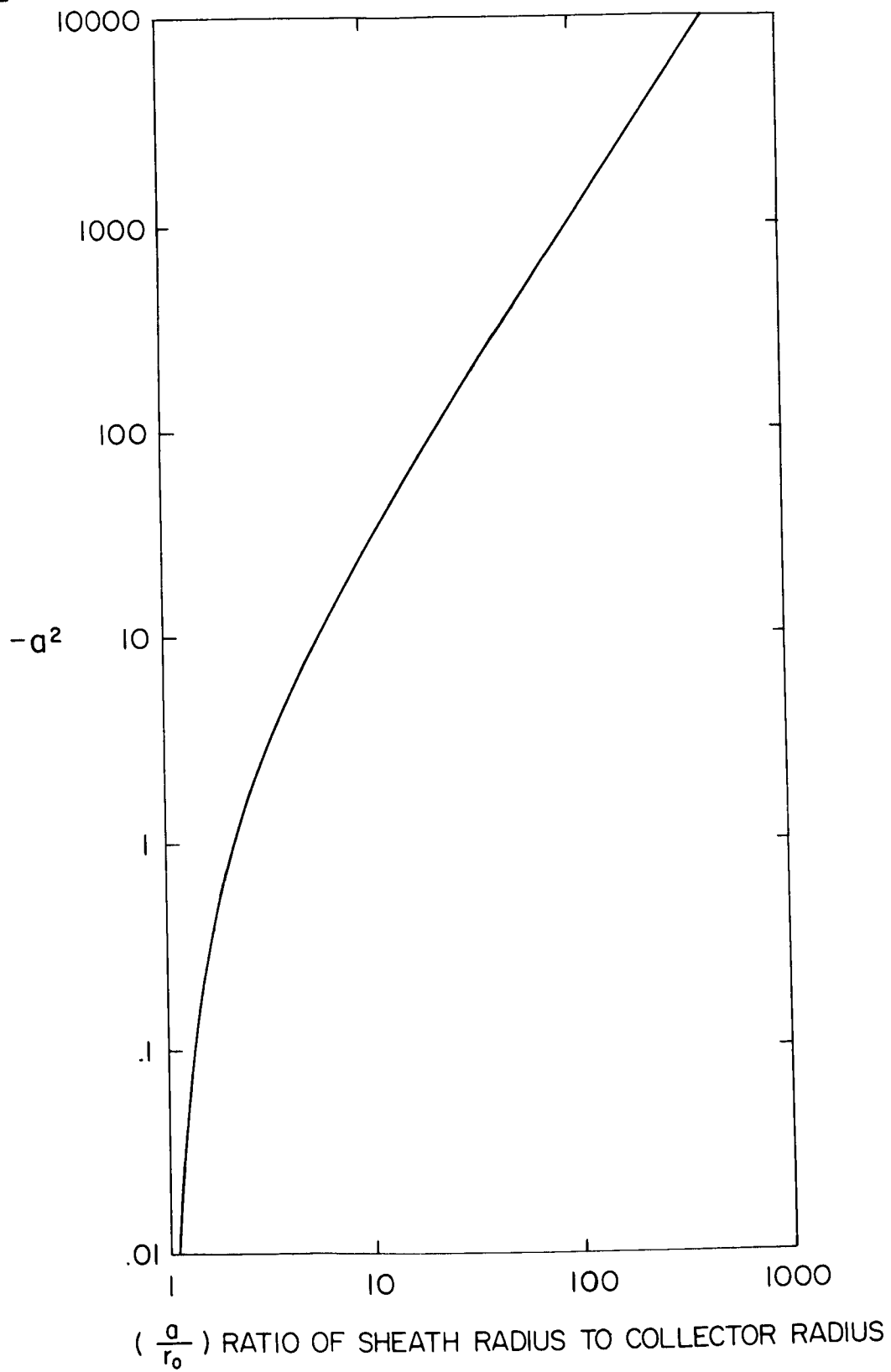


Figure 4.2 The quantity  $(-\alpha^2)$  arising in the theory of the spherical space-charge-limited diode.

in which  $A = \text{probe area} = 4\pi r_o^2$

$$J_r = \text{random ion current density} = Ne \sqrt{\frac{kT}{2\pi M}}.$$

The above equation gives the voltage-current curve but does not give any idea of the size of the probe's region of influence (or ion sheath). The sheath size can be estimated by calling upon the theory of the spherical space-charge-limited diode in which the outer electrode is the particle emitter and the inner electrode the particle collector. The sheath radius "a" is identified with the radius of the outer electrode and the following voltage-current relation deduced:

$$i = A J_r \frac{8\sqrt{\pi}}{9} \left(\frac{\lambda_D}{r_o}\right)^2 \left(\frac{eV_o}{kT}\right)^{3/2} \frac{1}{-\alpha^2} \quad (30)$$

The symbol  $\lambda_D$  indicates the Debye-Hückel shielding length whose variation with temperature and charged-particle density is displayed in Figure 4.1. The quantity  $(-\alpha^2)$  is a function of  $a/r_o$  and is shown in Figure 4.2. The elimination of  $i$  from (29) and (30) with the approximation  $\frac{eV_o}{kT} \gg 1$  gives

$$-\alpha^2 = \frac{8\sqrt{\pi}}{9} \left(\frac{\lambda_D}{r_o}\right)^2 \left(\frac{eV_o}{kT}\right)^{1/2}. \quad (31)$$

Given density, temperature and probe voltage one may deduce the sheath radius with the help of Figure 4.2.

#### 4.3.2 Validity of the Theory

The collisionless theory summarized above is called "orbital-motion-limited" (as opposed to "sheath-area-limited" for thin sheaths). The

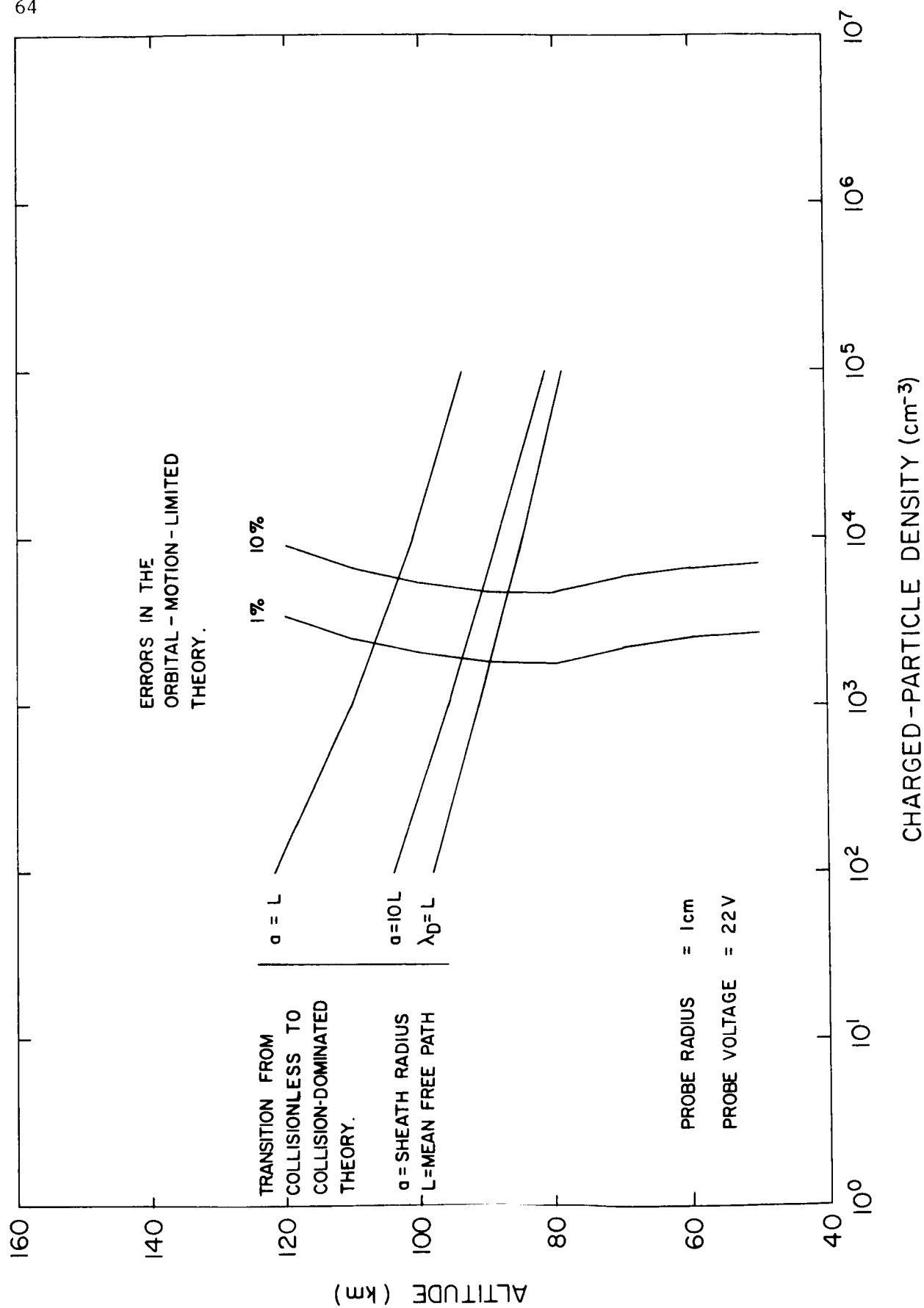


Figure 4.3 Validity limits for the theories.

orbital-motion-limited theory is accurate to about one percent provided  $T/nr_0^2 \geq 10^{-3}$  and accurate to about ten percent provided  $T/Nr_0^2 \geq 3 \times 10^{-4}$  (in MKS units). These criteria are plotted in Figure 4.3 for a 1 cm radius probe in the lower ionosphere.

The collisional theory discussed in the previous chapter depends for its validity on a mean free path which is short compared to the radius of influence of the probe. In particular, a criterion of "ten collisions in the sheath" has been employed by Schultz and Brown (1955). For a large value of  $a/r_0$  and a mean free path represented by  $L$ , this criterion may be stated as  $a = 10 L$ . For values of "a" derived from (31) and values of  $L$  taken from the U. S. Standard Atmosphere (1962) the criterion is plotted in Figure 4.3. Also included are plots of two other criteria,  $a = L$  and  $\lambda_D = L$ . These three collision criteria serve to indicate the transition region from collisional to collisionless ion motion with reference to a particular probe radius and voltage (1 cm and 22 volts in this case).

#### 4.3.3 High Pressure Velocity Dependence

As stated in the previous chapter, the dependence of ion drift velocity on electric field strength may be expressed as

$$v = \eta \left( \frac{E}{P_0} \right)^\beta. \quad (32)$$

The number  $\beta$  for atmospheric gases is approximately 0.6 for high  $E/P_0$  and 1.0 for low  $E/P_0$ . The transition between low-field and high-field conditions is at  $E/P_0 \approx 5 \times 10^3$  volts/m. - mm. H<sub>g</sub>. The problem now is to determine the altitude in the ionosphere at which this transition occurs.

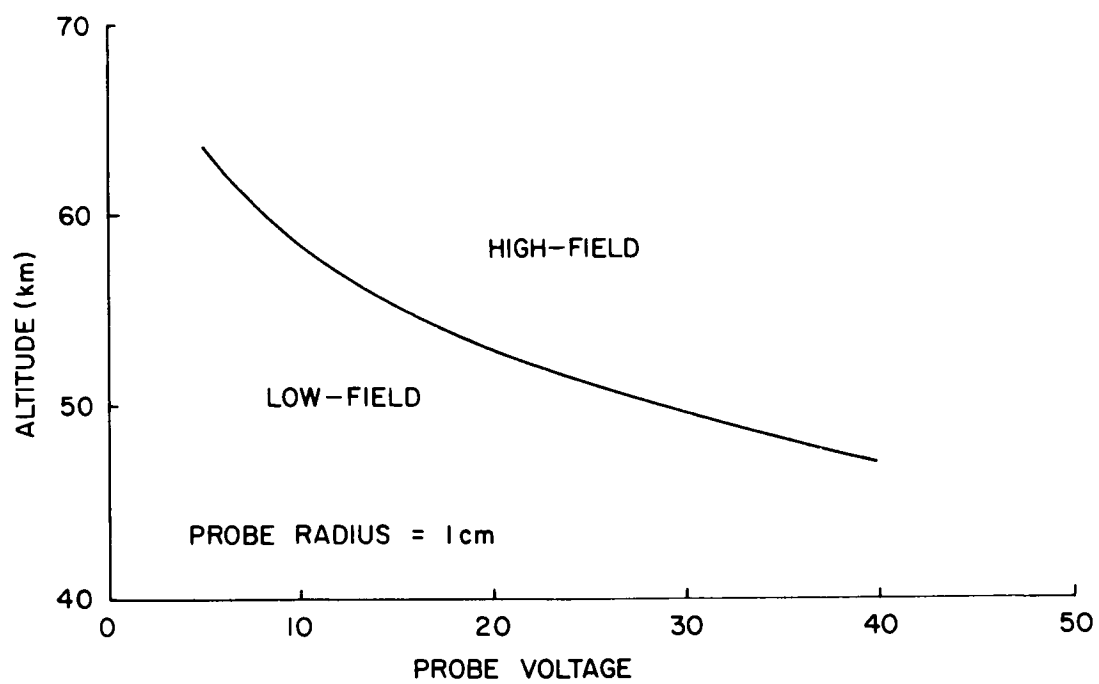


Figure 4.4 Altitude of transition from high-field to low-field ion motion.

In order to estimate the transition altitude it is necessary to know approximately the electric field of the probe at a given potential. This field may be approximated by the field of a spherical electrode in free space (realizing that the electric field strength in a plasma will be higher due to the shielding effect). If  $E_o$  is defined as the electric field strength at the probe surface, then the transition criterion becomes

$$E_o/P_o = 5 \times 10^3 \text{ volts/m.} - \text{mm.Hg.} \quad (33)$$

If  $V_o$  is the magnitude of the probe potential, then elementary electrostatics yields

$$E_o = V_o/r_o \quad (34)$$

Elimination of  $E_o$  from (33) and (34) and inclusion of the probe radius of  $10^{-2}$  m gives a transition pressure of

$$P_o = V_o/50 \text{ mm. Hg.} \quad (35)$$

The relation between pressure and altitude as given in the U. S. Standard Atmosphere (1962) permits the transition altitude to be plotted as a function of probe voltage as shown in Figure 4.4. Since altitudes above 50 km are of interest at present it is clear that high-field theory ( $\beta \approx 0.6$ ) is appropriate.

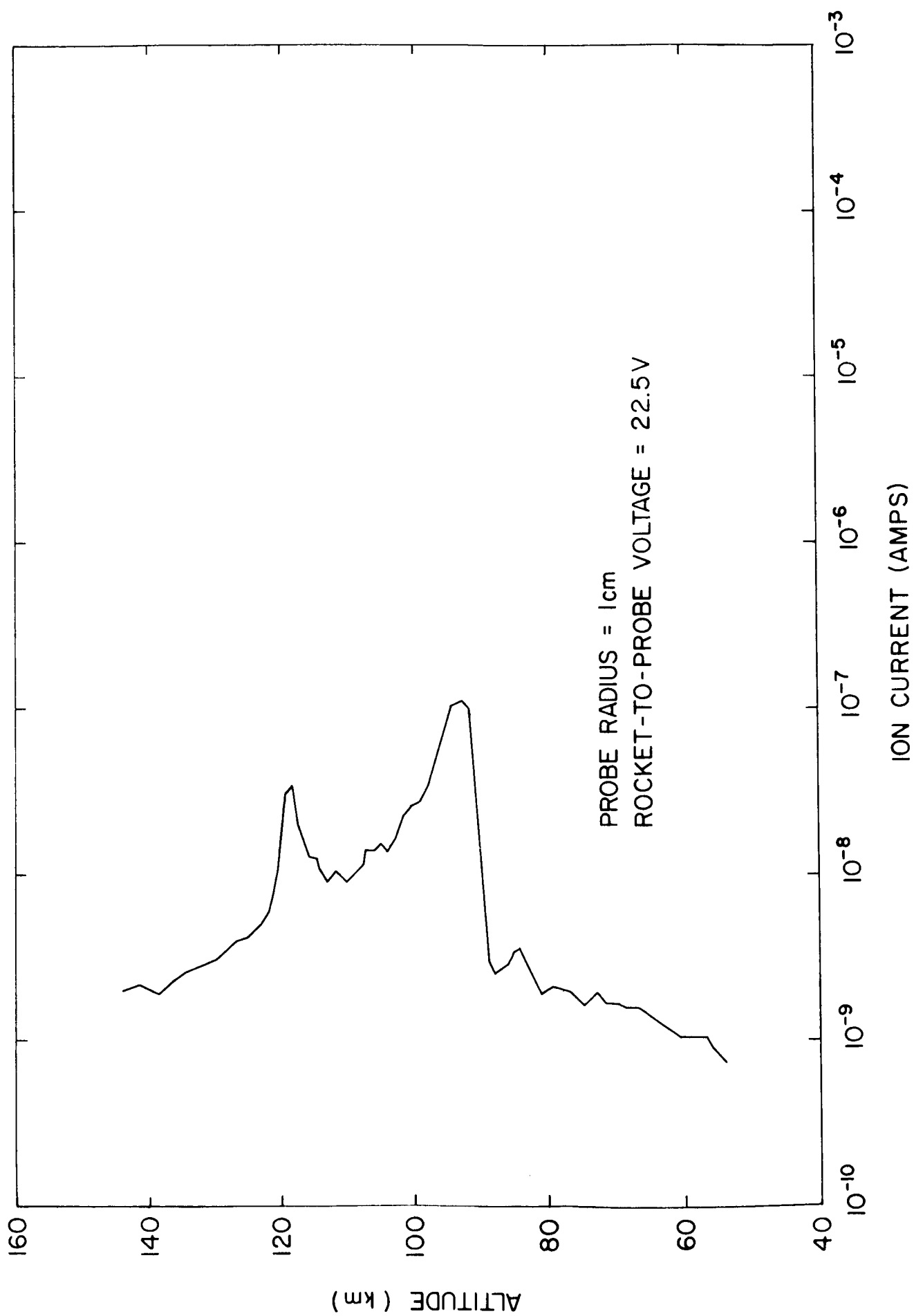


Figure 4.5 Measured ion current in the ionosphere.



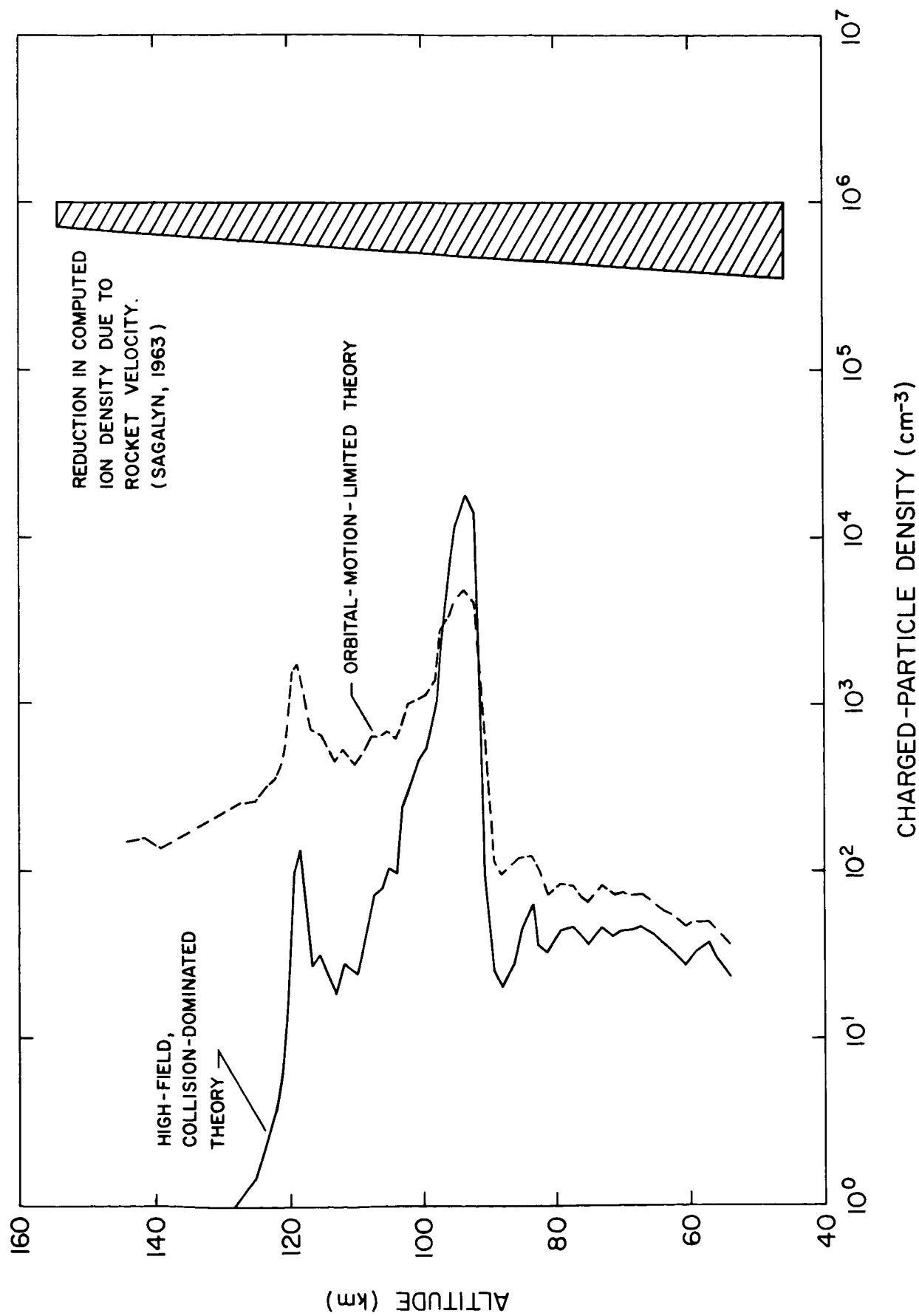


Figure 4.6 Ion density profiles.

Although high-field conditions prevail close to the probe, there must be a low-field region farther away from it. An analysis incorporating both low-field and high-field ion motion has not been carried out due to the complexity of the problem. However, since conditions close to a probe are most influential in determining the current, the use of high-field theory alone should produce a reasonably accurate solution.

#### 4.3.4 Results of Pre-sunrise Rocket Flight 14.144 at Wallops Island, Virginia

The measured ion current to a spherical probe is shown in Figure 4.5. The measurements are for ascent and the launch took place at 0300 EST on July 15, 1964. The ion current was measured at a fixed negative potential of 22.5 volts.

The ion density profile using the high-field collisional theory is shown in Figure 4.6. For this computation, the values  $\beta = 0.6$  and  $\gamma = 3.45$  (MKS units) were obtained from McDaniel (1964). These are values for  $N_2^+$  ions in  $N_2$  and they are probably approximately correct for the  $NO^+$  ions believed to predominate in the lower ionosphere. This choice of constants results in the following formula which was used to compute the ion density profile:

$$N = 1.08 \times 10^{25} \left(\frac{273}{T}\right)^{1.046} p^{.546} i^{1.91} \text{ ions/m}^3. \quad (36)$$

The criteria plotted in Figure 4.3 indicate that this formula is valid below about 90 km. It is interesting to note that the positive ion density between 54 and 89 km is nearly constant at about 40 ions per cc., a density which is consistent with VLF measurements in the "C-layer" at sunrise

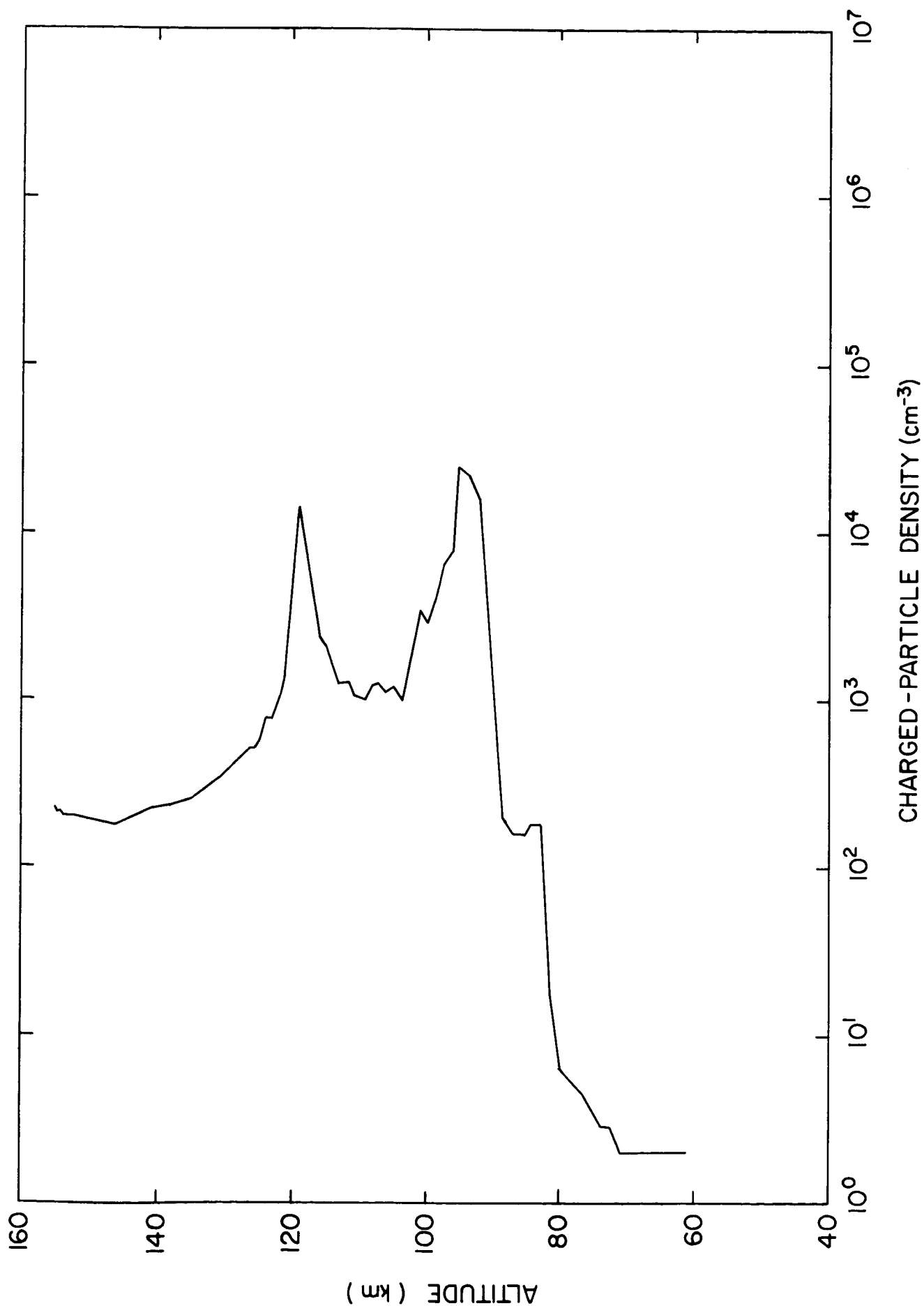


Figure 4.7 Electron density as measured by conical nose probe.

(Sechrist, 1965). Additional profiles (not shown) were plotted for  $\beta = .5$  and  $\beta = 1.0$ ; these yielded ion densities respectively less and greater (than those shown) by factors of about four. Clearly the predicted ion density is strongly dependent on the relation between drift velocity and electric field strength. Also included in Figure 4.6 is a correction factor derived by Sagalyn and Smiddy (1963); it is not certain at present that this correction is applicable to the ion density profiles derived from high-field theory.

Above 110 km collisionless orbital-motion-theory is applicable and the current-voltage relation is given in (29). In this case  $V_0 = 22$  volts and thus  $\frac{eV_0}{kT} \gg 1$ . With this approximation, the ion density is

$$N = 4.69 \times 10^{16} \sqrt{T/273} \text{ i ions/m}^3 \quad (37)$$

for  $N_2^+$  ions and a probe of 1 cm radius. A graph of (37) is shown in Figure 4.6; this profile intersects the one predicted by (36) at 91 km and 97 km. Both of these intersections are in the range of altitudes in which the ion motion changes from collisionless motion to collision-dominated motion.

Shown in Figure 4.7 is an electron density profile derived from the voltage-current characteristic of a conical probe consisting of a six-inch section at the top of the rocket nose cone. The profile was supplied by L. G. Smith of GCA Corporation. The difference between the electron density profile and the ion density profile below 80 km presumably indicates the presence of negative ions.

#### 4.3.5 Zero Space Charge Theory

The collision-dominated ion collection theory discussed and applied up to this point makes use of the experimentally determined variation of ion velocity with electric field and takes into account the presence of space charge. In order to estimate the importance of including space charge, one may attempt to formulate a theory which neglects it. Neglect of space charge implies that the probe field in a plasma is the same as in free space. That is,

$$V = \frac{Q}{4\pi\epsilon r} \quad (38)$$

$$E = \frac{Q}{4\pi\epsilon r^2} \quad (39)$$

in which  $Q$  is the charge on the probe. The requirement of constant total current " $i$ " at all radii produces the relation

$$i = nev \, 4\pi r^2 \quad (40)$$

from which arises the restriction

$$nv \propto r^{-2} \quad (41)$$

in which  $n$  is the ion density. Space charge neutrality requires that the positive ion density  $n$  be cancelled out by a background of electrons and negative ions. Frequently it is assumed that the charged particle density is unaffected by the presence of the probe; this would permit the replacement of  $n$  by  $N$  which is a constant. This assumption in turn imposes the restriction

$$v \propto r^{-2} \quad (42)$$

or

$$v \propto E \quad (43)$$

which immediately rules out high-field ion motion. Thus, zero space charge theory cannot be applied to the rocket probe except possibly in the vicinity of 50 km. With  $\beta = 1$ , (32) permits the derivation of the following current-voltage relation

$$i = \frac{4\pi N_e n r_o}{P_o} V_o . \quad (44)$$

Equation (44) displays a linear relation between current and voltage and provides a means of computing ion density. The ion density computed using the above formula is  $5 \times 10^3$  ions/cc at 54 km which is more than two orders of magnitude greater than either the collisional or collisionless result (both approximately 40 ions/cc). It must be concluded that space charge is important even under low-field conditions.

#### 4.4 Probe Measurements in the Laboratory

Testing the high-pressure probe theory in the laboratory is difficult due to the requirement that the sheath radius be much larger than the probe radius. For a 1/8" diameter probe this means that the charged-particle density in the laboratory discharge tube must be in the vicinity of  $10^6$  to  $10^7$  per cc. The range of densities which can be obtained easily in steady state laboratory discharges is about  $10^9$  to  $10^{10}$  per cc with a range from  $10^8$  to  $10^{11}$  per cc available with some difficulty. The difficulties referred to are discharge current drift and plasma non-uniformity at low densities and overheating at high densities.

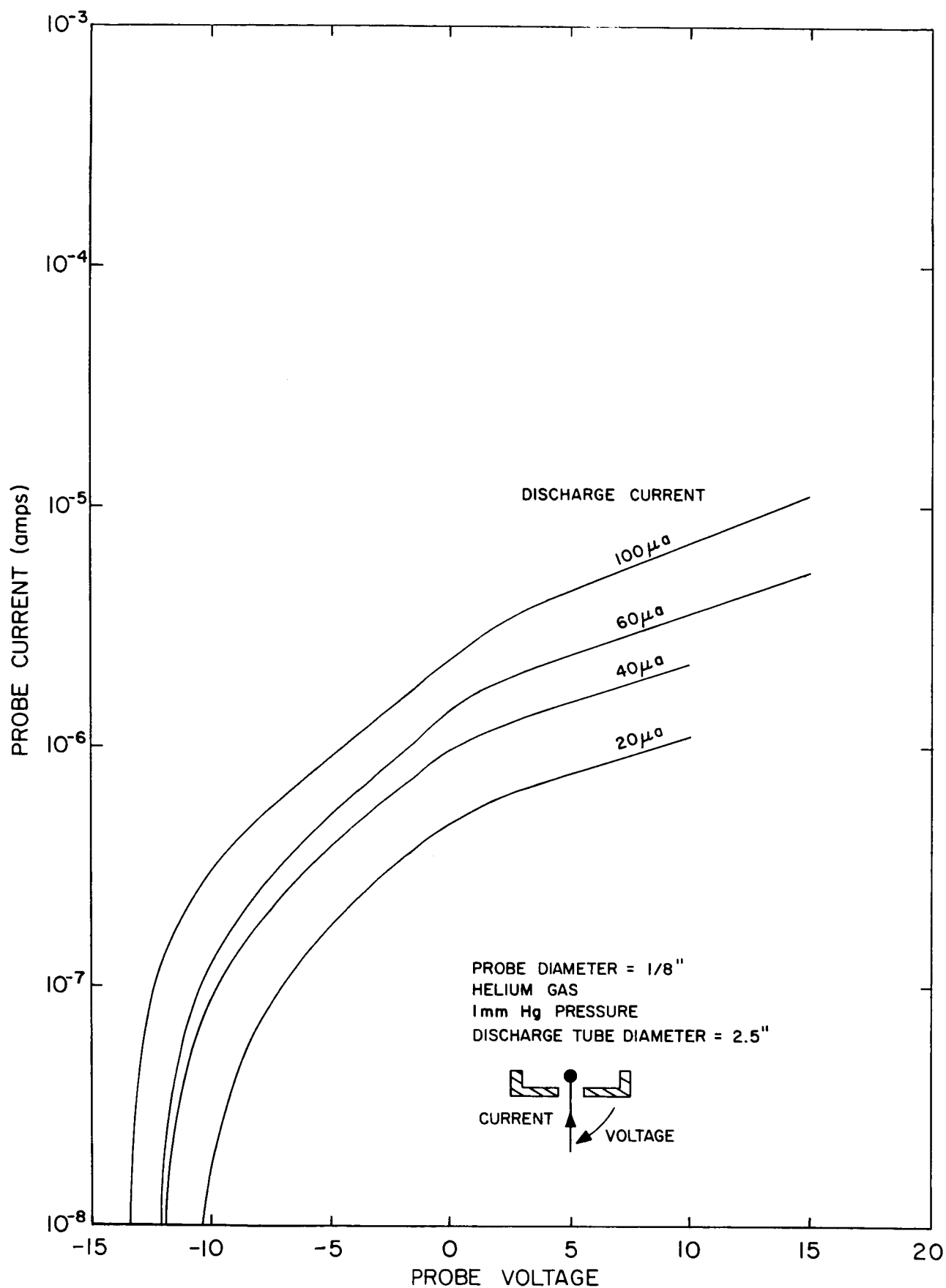


Figure 4.8 Electron-collection curves for a spherical probe in a laboratory plasma.

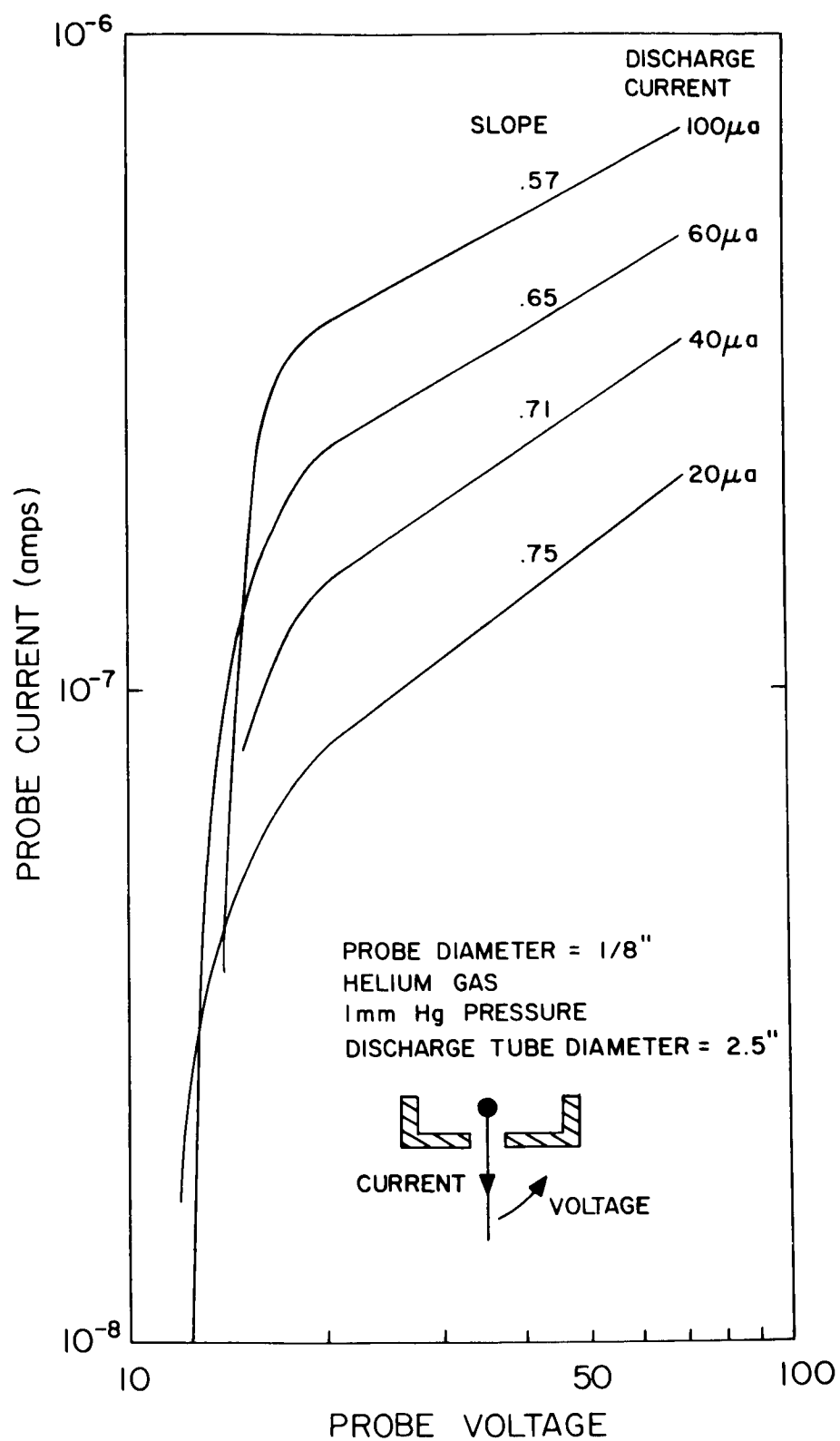


Figure 4.9 Ion-collection curves for a spherical probe in a laboratory plasma.



Despite the difficulty in working at low charged-particle densities an experiment was carried out using a 1/8" diameter spherical probe in a brush cathode discharge tube which has been described in detail by Kostelnicek (1965). Helium gas at 1 mm pressure was used, a combination which produced an electron density of  $10^8$  per cc with a discharge current of 1 ma. Probe voltage-current curves were taken at four values of discharge current in the range 20  $\mu$ a to 100  $\mu$ a as shown in Figures 4.8 and 4.9. The electron-collection curves in Figure 4.8 are sufficiently unlike the classical Langmuir probe characteristic that they cannot be used to deduce electron temperature and density. However, the ion-collection curves in Figure 4.9 become straight lines in the log-log graph, indicating that the current is proportional to the voltage raised to some power given by the slope of the line. This is exactly the behavior predicted by (25) and the slope on the log-log graph should be  $2(1 + \beta) (3 + 2\beta)^{-1}$ . Under high-field conditions in helium,  $\beta = 1/2$  and the predicted slope is .75. The curves have slopes which increase with decreasing discharge current, a slope of .75 being reached at the lowest discharge current, 20  $\mu$ a.

The expected electron density at a discharge current of 20  $\mu$ a is about  $2 \times 10^6$  per cc, based on the assumption that the electron density is proportional to the discharge current and extrapolating from  $10^8$  per cc at 1 ma. However, the ion density can be calculated much more precisely from the probe current using (28). Assuming an ion temperature of 300°K (which is probably too low) and deducing  $\eta = 4.0$  MKS units from Brown (1959), the calculated ion density is  $3.2 \times 10^6$  per cc which is close to the estimated value of  $2 \times 10^6$  per cc. The sheath radius calculated from (24) is 7.64 mm

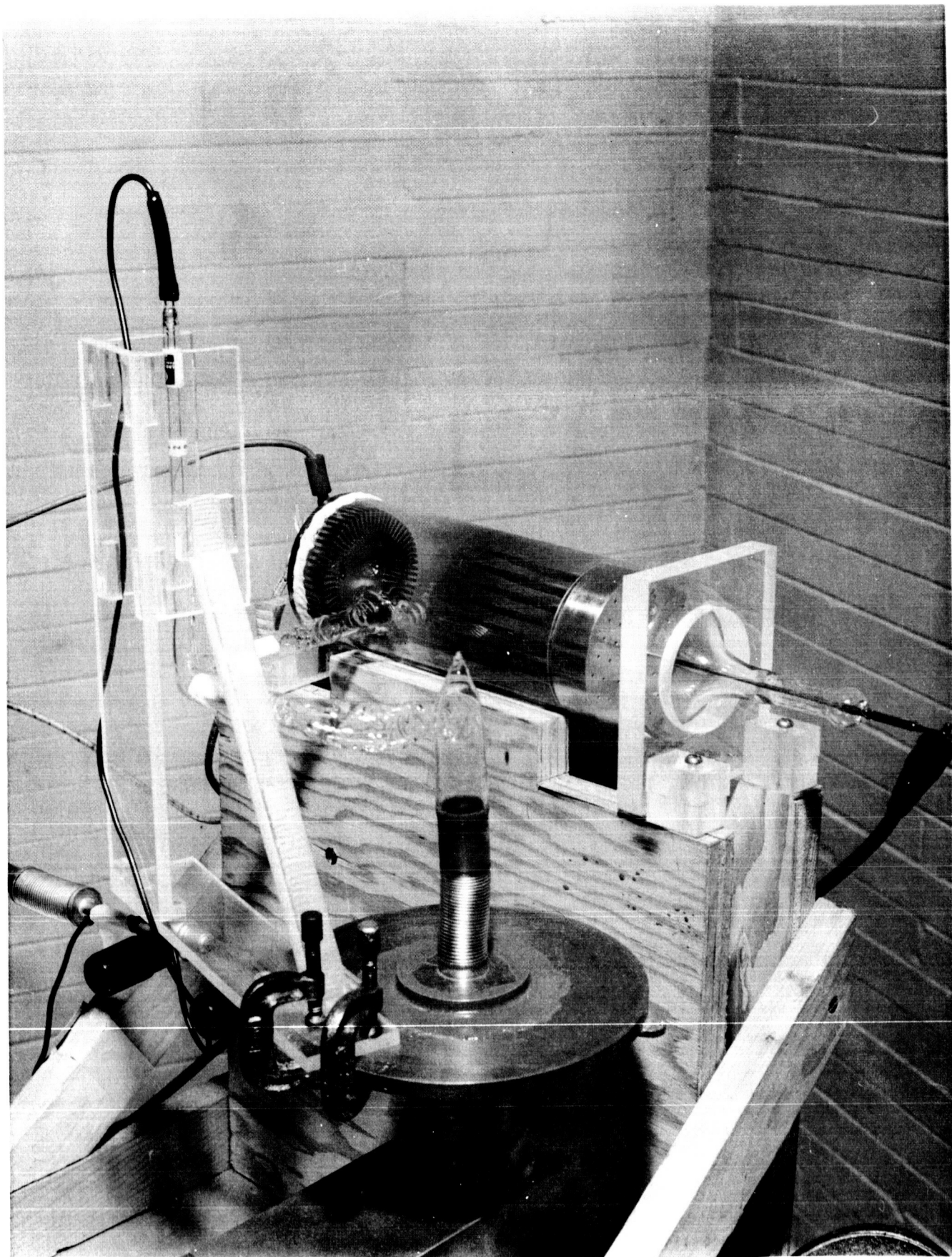


Figure 4.10 Laboratory gas discharge apparatus.

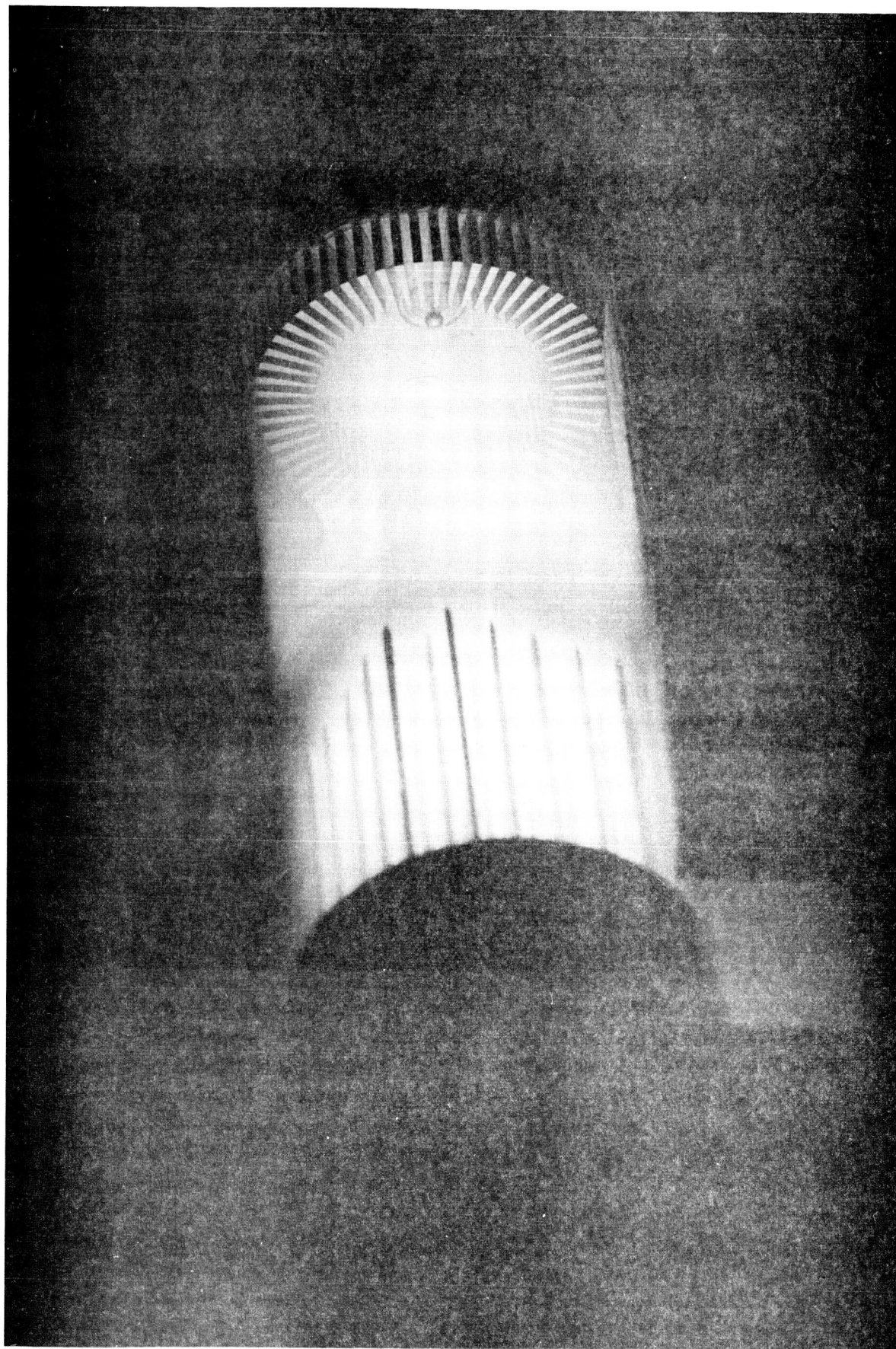


Figure 4.11 Brush cathode discharge tube with spherical probes.

and the probe radius is 1.59 mm, giving  $a/r_0 = 4.8$ , a value which satisfies fairly well the condition  $a/r_0 \gg 1$ . An equally important condition is that there must be many collisions in the sheath. At a pressure of 1 mm Hg, the mean free path in helium is 0.5 mm and in the above example the sheath thickness is 5 mm. This indicated ten collisions in the sheath and thus the collision condition is satisfied. The above calculations suggest that the spherical probe theory derived in this report can be very useful in the diagnosis of low-density plasmas. Furthermore, it has been shown that the brush cathode laboratory discharge tube can be used to obtain charged-particle densities as low as  $10^6$  per cc.

The laboratory gas discharge apparatus is shown in Figure 4.10. The tungsten spikes forming the brush cathode are clearly visible through the glass which has been darkened by metal sputtered off the cathode. The two small spherical probes may be seen at the other end of the tube. They are surrounded by the finned anode, the fins being necessary to provide enough anode area for Langmuir probe measurements. Figure 4.11 shows the same discharge tube in operation.

## 5. FUTURE IONOSPHERIC PROBE EXPERIMENTS

### 5.1 Introduction

Both DC and RF probes have been used on rockets and satellites for several years but in many cases the experimental results have been very difficult to interpret. For instance, in the case of RF impedance probes, the experimental results have required corrections for the ion sheath and electroacoustic radiation and, furthermore, there has been much inconclusive discussion about the effect of DC bias. In addition, early resonance probe experiments produced puzzling results such as the complete disappearance of the rectified current peak. It would appear that many of these difficulties arose because the experiments were designed primarily to measure geophysical quantities rather than being designed to study the probe-plasma interaction itself. Thus in retrospect one may conclude that programs of laboratory and ionospheric probe studies should have preceded geophysical measurements.

At the present time it is clearly desirable to carry out an experimental study designed specifically to fill in some of the "gaps" in the understanding of probe behavior. Laboratory plasma experiments offer the distinct advantage of accessibility but for some experiments, the ionospheric plasma is definitely preferable. For instance, RF resonance effects are easy to recognize in the ionosphere because of the low value of  $\frac{\nu}{\omega_N}$ , the ratio of the collision frequency to the plasma frequency. In laboratory plasmas it is very difficult to obtain a value of  $\frac{\nu}{\omega_N}$  as low as  $10^{-2}$  due to the difficulty in maintaining a low-pressure discharge. However, in the ionosphere  $\frac{\nu}{\omega_N} \approx 10^{-2}$  at an altitude of 100 km and  $\frac{\nu}{\omega_N} \approx 10^{-4}$  at 300 km. Thus at the higher altitudes (in the F-region), the ionosphere is well suited for studies of plasma resonances and instabilities.

An important factor in probe studies is the uniformity of the plasma adjacent to the probe when it is biased to space potential; it is this bias level at which the electron density is determined using DC probe techniques. if  $n_p$  is the electron density at the surface of a spherical probe of radius  $R$ ,  $N$  is the ambient electron density and  $\lambda$  is the electron mean free path, then according to Wasserstrom et al. (1965),

$$\frac{n_p}{N} = \frac{1}{2(1 + \frac{R}{\lambda})}.$$

It is evidently necessary to require the condition  $R/\lambda \ll 1$  in order to minimize plasma non-uniformity. In laboratory plasmas, typical maximum values of  $\lambda$  are 1 cm in neon and 1 mm in helium while in the ionosphere  $\lambda \approx 1$  m at 100 km and  $\lambda \approx 100$  m at 300 km. Thus the condition  $R/\lambda \ll 1$  would be easier to achieve in the ionosphere. Of course this simple picture neglects entirely the Earth's magnetic field.

The influence of the Earth's magnetic field can be estimated by noting that the electron gyroradius  $r_g$  varies from 0.6 cm at 100 km to 3 cm at 300 km. Thus  $r_g$  is likely to be of the same order of magnitude as the dimensions of the probe (such as  $R$ , the spherical probe radius). Much more important than  $r_g/R$ , however, is the ratio of  $r_g$  to the Debye length  $\lambda_D$ , large values of  $r_g/\lambda_D$  indicating that the magnetic field will have little effect on a DC probe characteristic. The ratio  $r_g/\lambda_D$  varies from 0.5 at 100 km to 15 at 300 km, a range which goes all the way from a strong to a weak magnetic field effect. As far as RF probes are concerned, the influence of the magnetic

field is very roughly proportional to  $\omega_H/\omega_N$ , the ratio of the gyrofrequency to the plasma frequency. At 100 km  $\omega_H/\omega_N \approx 1$ , indicating a strong effect, while at 300 km  $\omega_H/\omega_N \approx 0.1$ , indicating a weak effect. These examples all lead to the conclusion that DC and RF probes would experience little magnetic field effect near the F-region peak in electron density but that this effect could become strong at lower or higher altitudes.

In recent years it has been shown theoretically that the compressibility of the electron gas can influence the behavior of an RF probe. It has been predicted that this compressibility will cause the radiation of electroacoustic waves and will change the probe impedance appreciably. The various theories all have one point in common, that compressibility effects are strong if the probe dimensions (radii of curvature, gap width, etc.) are comparable to a Debye length and weak if the dimensions are much greater than  $\lambda_D$ . In the ionosphere,  $\lambda_D$  varies from 1.2 cm at 100 km to 2 mm at 300 km so that compressibility effects may be made either large or small according to the design of the probe and the choice of altitude.

## 5.2 Experimental Techniques

### 5.2.1 Langmuir Probe

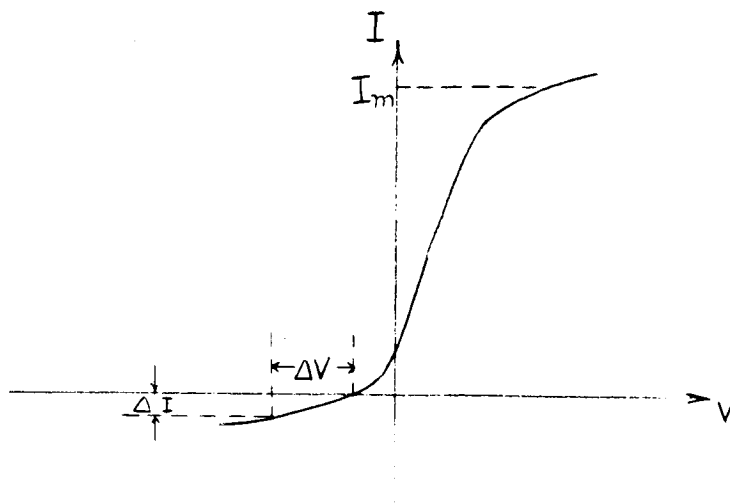
Langmuir or DC probe experiments must be regarded as fundamental in a rocket program because these experiments lead to values of space potential, electron temperature and electron density; thus the first objective must be to obtain a good Langmuir probe current-voltage curve. Unfortunately, this is not easy to do as many laboratory and ionospheric experiments have demonstrated. Recent experiments in the Aeronomy Laboratory have brought to prominence the necessity for clean probe surfaces. The required cleanliness



was achieved only after a brief period of ion bombardment in the pure, low-pressure gas atmosphere to be used in the experiment. This cleaning procedure appreciably reduced the apparent electron temperature and completely removed irregularities which had made the current-voltage curve extremely difficult to interpret. In a rocket, cleaning could be accomplished by applying several hundred volts (both positive and negative) for a few seconds between the probe and the rocket body or between the two halves of an electrically "split" rocket body so that all metal surfaces are exposed to the cleaning process. At present it is not known if the ion density in the ionosphere would be sufficient for cleaning or if additional ionization would be necessary; probably the best experimental approach would be to use as high a voltage as possible in series with a current-limiting resistor. The additional ionization caused by the cleaning process might temporarily degrade or even interrupt telemetry transmission so that preparations would have to be made for such an eventuality. A good experimental sequence would consist of two or three cleaning operations interspersed between DC probe curves. Careful sealing of the rocket body and motor casing would be necessary to avoid the evolution of contaminant gases.

A further requirement for a good DC probe characteristic is a large ratio of reference electrode area to probe area. The larger this ratio is, the smaller is the change in voltage between the plasma and the reference electrode during a probe experiment. This voltage change  $\Delta V$  can be predicted approximately from a typical current-voltage curve as shown in the accompanying diagram.





$$\Delta I = I_m \frac{(\text{Probe area})}{(\text{Rocket Area})}$$

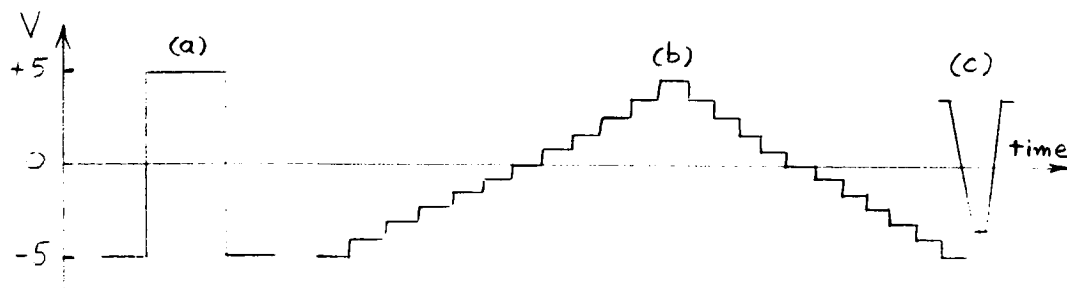
Here, the rocket is taken to be the reference electrode.

From laboratory experiments, if the maximum allowable  $\Delta V$  were 0.1 volt, then the required area ratio would be (Reference electrode area)/(Probe area)  $\approx 1000$ .

### 5.2.2 Transient Response

One of the most important rocket experiments involves the measurement of the time required for a DC probe to respond to a change in applied voltage.

In general, two response times are of interest, the "overall" response time required for a complete probe curve and the "incremental" response time applicable at any point on the curve. Three suggested waveshapes for the applied voltage are sketched below.



In (a), an overall response time would be the quantity measured, while in (b) it would be an incremental response time. Waveform (c) would serve to reveal hysteresis effects. Expected response times would be at least as great as one period at the ion plasma frequency (say one to ten milliseconds). Diffusion effects might extend this time considerably and thus laboratory measurements of response time would be advisable prior to the design of rocket instrumentation. In addition, the use of a probe current amplifier with a logarithmic response would permit reading time constant, electron density and electron temperature directly from the telemetry records.

### 5.2.3 Impedance Probe

A considerable body of theoretical work on probe impedance is available at present and ionospheric experiments are needed in order to check the theory. A well-designed impedance experiment would involve swept-frequency impedance (admittance) measurements carried out at several pre-set bias voltages. A useful F-region frequency range would be from half the electron gyrofrequency to twice the electron plasma frequency. In impedance measurements it is important to keep the RF voltage low; a satisfactory peak voltage would be about  $1/2 \cdot \frac{kT}{e}$  or .05 volts at 1200°K and a continuous monitoring of the rectified current to the probe would reveal any non-linear tendencies. The unavoidable variations in rocket attitude would provide a continuous change in probe orientation with respect to the magnetic field. If probe dimensions were kept small (comparable to  $\lambda_D$ ), it would be possible to observe impedance effects caused by the compressibility of the electron gas; the physical existence of these effects is not yet well established.

Impedance effects to be observed include resonances of the plasma medium such as the common magneto-ionic theory resonances and also the cyclotron-harmonic responses as observed with the Alouette satellite. Some resonances occur at frequencies which are dependent on the size of the ion sheath (i.e. the series resonance which can occur between the capacitive sheath and an inductive plasma); these resonances can be identified by the dependence of the resonant frequency on probe bias. In addition to resonances, one might look for the high losses associated with "hyperbolic" conditions (Balmain, 1964; Hodges, 1964). This phenomenon would appear as a bias-independent "jump" in the real part of the probe impedance or admittance.

#### 5.2.4 Resonance Probe (Resonance Rectification)

This resonance experiment is similar to the impedance experiment already described. The only requirement would be the increase in RF voltage to a peak value between  $3 \frac{kT}{e}$  and  $4 \frac{kT}{e}$  (as has been determined by laboratory experiment); in a rocket, two or three different RF levels might be employed. In this experiment it is important that the RF voltage at the probe be kept constant during the frequency sweep. The optimum DC bias point is at the ion saturation "knee" in the Langmuir probe curve (Kostelnicek, 1965).

#### 5.2.5 Probe Configurations

The shape of a probe determines how the measured quantities will vary with rocket attitude. Measurements on a small spherical probe (1 to 5 cm radius) mounted on the nose of the rocket should be nearly independent of attitude. A cylindrical dipole configuration (2 to 4 m long) would be a good choice for studying the influence of the Earth's magnetic field. A

segmented sphere would be helpful in studies of photoemission and flow effects. Photoemission might also be studied by the use of a small spherical probe mounted a short distance from the side of the rocket--the presence of photoemission would cause a change in the measured quantity as the probe passes from the sunlight into the shadow of the rocket.

### 5.3 Experimental Program

The first experiments should be carried out near the F-region peak in electron density since the magnetic field effects are secondary there and the electron density can be determined both from "bottomside" and "topside" sounding techniques. Later experiments designed to explore magnetic field effects could be carried out at lower or higher altitudes. At the lower altitudes, "heating" radio waves might be transmitted from the ground and the rocket equipment employed to look for wave-plasma interactions. Another extension of the work would involve measurement of mutual impedance between two antennas or measurement of the interaction between pairs of experiments carried on the same vehicle.

## REFERENCES

- Aono, Y., K. Hirao and S. Miyazaki (1962), Rocket observation of ion density, electron density and electron temperature in the ionosphere, J. Rad. Res. Labs. 9, No. 46, 407-420.
- Balmain, K. G. (1964), The impedance of a short dipole antenna in a magnetoplasma, IEEE Trans. on Antennas and Propagation, Vol. 12, 605-617.
- Balmain, K. G. (1965), Impedance of a short dipole in a compressible plasma, Radio Sci. J. Res. NBS/USNC-URSI 69D, No. 4, 559-566.
- Bhatnagar, P. L., E. P. Gross, and M. Krook (1954), A model for collision processes in gases. I. Small amplitude processes in charged and neutral one-component systems, Phys. Rev. 94, No. 3, 511-525.
- Bogges, R. L. (1959), Electrostatic probe measurements of the ionosphere, Scientific Report No. G.S.-1, Space Physics Research Laboratory, University of Michigan, Ann Arbor, Michigan.
- Brown, S. C. (1959), Basic data of plasma physics, Massachusetts Institute of Technology Press, Cambridge, Massachusetts.
- Crawford, F. W. (1965), Plasma resonance probe characteristics in a magnetic field, J. Appl. Phys., 36, 3142-3145.
- Crawford, F. W. and R. S. Harp (1965), The resonance probe--a tool for ionospheric and space research, J. Geophys. Res. 70, No. 3, 587-596.
- Crawford, F. W. and R. F. Mlodnosky (1964), Langmuir probe response to periodic waveforms, J. Geophys. Res. 69, No. 13, 2765-2773.
- Cohen, M. H. (1961), Radiation in Plasmas, Part I, Phys. Rev. 123, No. 3, 711-721.
- Cohen, M. H. (1962), Radiation in Plasmas, Part II and Part III, Phys. Rev. 126, No. 2, 389-397, 398-404.
- Dote, T. and T. Ichimiya (1965), Characteristics of resonance probes, J. Appl. Phys. 36, 1866-1872.
- Fejer, J. A. (1964), The interaction of an antenna with a hot plasma and the theory of resonance probes, Radio Sci. J. Res. NBS/USNC-URSI 68D, No. 11, 1171-1176.
- Hall, R. B. (1963), Parallel plate plasma problem, Am. J. Phys. 31, No. 9, 696-706.

- Harp, R. S. and F. W. Crawford (1964), Characteristics of the plasma resonance probe, J. Appl. Phys. 35, No. 12, 3436-3446.
- Hessel, A., N. Marcuvitz, and J. Shmoys (1962), Scattering and guided waves at an interface between air and a compressible plasma, IEEE Trans. on Antennas and Propagation, Vol. 10, No. 1, 48-54.
- Hodges, R. R., Jr. (1964), Gyro-interaction rocket experiments in the lower ionosphere, University of Illinois Aeronomy Report No. 3.
- Jones, D. S. (1964), The theory of electromagnetism, Pergamon Press, MacMillan Co., New York.
- Kaiser, T. R. (1962), The admittance of an electric dipole in a magneto-ionic environment, Planet. Space Sci. 9, 639-657.
- Kostelnicek, R. J. (1965), The admittance and resonance probe characteristics of a spherical plasma probe, University of Illinois Aeronomy Report No. 8.
- Langelier, R. M. (1964), Radiation from a vertical electric dipole in a warm plasma above a conducting plane, Ph.D. Thesis, Purdue University, Lafayette, Indiana.
- Lees, L. (1959), A kinetic theory description of rarefied gas flows, Hypersonic Research Project Memorandum No. 51, Guggenheim Aeronautical Laboratory, California Institute of Technology.
- Lees, L. (1965), Kinetic theory description of rarefied gas flow, J. Soc. Indust. Appl. Math. 13, No. 1, 278-311.
- Lees, L. and C.-Y. Liu (1962), Kinetic-theory description of conductive heat transfer from a fine wire, Phys. of Fluids 5, No. 10, 1137-1148.
- Liu, C.-Y. and L. Lees (1961), Kinetic theory description of plane compressible couette flow, Rarefied Gas Dynamics (Advances in Applied Mechanics, Supplement 1), Academic Press, Inc., New York, 391-428.
- McDaniel, E. W. (1964), Collision phenomena in ionized gases, John Wiley & Sons, Inc.
- Mlodnosky, R. F. and O. K. Garriott (1962), The VLF admittance of a dipole in the lower ionosphere, Proc. of the International Conf. on the Ionosphere (Institute of Physics and Physical Society, London), 484-491.
- Mott-Smith, H. M. (1954), A new approach in the kinetic theory of gases, Lincoln Laboratory Group Report V-2, Massachusetts Institute of Technology.

- Pavlovich, J. M. (1964), Numerical calculations related to the RF properties of the plasma sheath, Report No. ARL 64017, Aerospace Research Laboratories, Office of Aerospace Research, U. S. Air Force.
- Sagaly, R. C. and M. Smiddy (1963), Theory of electrostatic probes for study of D-region ionization, University of Illinois Aeronomy Report No. 1, 22-25.
- Schulz, G. J. and S. C. Brown (1955), Microwave study of positive ion collection by probes, Phys. Rev. 98, No. 6, 1642-1649.
- Sechrist, C. F. (1965), Private communication.
- Seshadri, S. R. (1964), Radiation from an electromagnetic source in a half-space of compressible plasma-surface waves, IEEE Trans. on Antennas and Propagation, Vol. 12, No. 3, 340-348.
- Spitzer, L. (1962), Physics of fully ionized gases, Interscience Publishers Division of John Wiley and Sons, Inc., New York.
- U. S. Standard Atmosphere (1962), Available from the Supt. of Documents, U. S. Government Printing Office, Washington 25, D. C.
- Wait, J. R. (1964), Theory of a slotted-sphere antenna immersed in a compressible plasma, Parts I and II, Radio Sci. J. Res. NBS/USNC-URSI 68D, No. 10, 1127-1136, 1137-1143.
- Wasserstrom, E., C. H. Su, and R. F. Probstein (1965), Kinetic theory approach to electrostatic probes, Phys. of Fluids, 8, No. 1, 56-72.